

# A rotary molecular motor that can work at near 100% efficiency

Kazuhiko Kinosita Jr.<sup>1,2\*</sup>, Ryohei Yasuda<sup>2</sup>, Hiroyuki Noji<sup>2</sup> and Kengo Adachi<sup>2,3</sup>

<sup>1</sup>Department of Physics, Faculty of Science and Technology, Keio University, Hiyoshi, Kohoku-ku, Yokohama 223-8522, Japan

<sup>2</sup>Core Research for Evolutional Science and Technology—'Genetic Programming' Team 13, Teikyo University Biotechnology Center 3F, Nogawa, Miyamae-ku, Kawasaki 216-0001, Japan

<sup>3</sup>Department of Physics, Faculty of Science, Kanazawa University, Kakuma-machi, Kanazawa 920-11, Japan

A single molecule of  $F_1$ -ATPase is by itself a rotary motor in which a central  $\gamma$ -subunit rotates against a surrounding cylinder made of  $\alpha_3\beta_3$ -subunits. Driven by the three  $\beta$ s that sequentially hydrolyse ATP, the motor rotates in discrete  $120^\circ$  steps, as demonstrated in video images of the movement of an actin filament bound, as a marker, to the central  $\gamma$ -subunit. Over a broad range of load (hydrodynamic friction against the rotating actin filament) and speed, the  $F_1$  motor produces a constant torque of *ca.* 40 pN nm. The work done in a  $120^\circ$  step, or the work per ATP molecule, is thus *ca.* 80 pN nm. In cells, the free energy of ATP hydrolysis is *ca.* 90 pN nm per ATP molecule, suggesting that the  $F_1$  motor can work at near 100% efficiency. We confirmed *in vitro* that  $F_1$  indeed does *ca.* 80 pN nm of work under the condition where the free energy per ATP is 90 pN nm. The high efficiency may be related to the fully reversible nature of the  $F_1$  motor: the ATP synthase, of which  $F_1$  is a part, is considered to synthesize ATP from ADP and phosphate by reverse rotation of the  $F_1$  motor. Possible mechanisms of  $F_1$  rotation are discussed.

**Keywords:** molecular motor;  $F_1$ -ATPase; ATP synthase; energy conversion efficiency

## 1. INTRODUCTION

Molecular motors generate movement and force between two cellular components. Linear motors produce movement along a filamentous structure; for example, myosin along an actin filament (Goldman 1998; Suzuki *et al.* 1998; Dominguez *et al.* 1998; Kitamura *et al.* 1999), kinesin (Block 1998; Lohman *et al.* 1998; Mandelkow & Johnson 1998) and dynein (Shingyoji *et al.* 1998) along a microtubule, and RNA polymerase along DNA (Gelles & Landick 1998; Wang *et al.* 1998). Known linear motors are driven by free energy obtained from nucleotide hydrolysis. Usually, the molecule that contains the hydrolysis site(s), excluding the filament, is called a motor and the filament is regarded as a track, although the filament is likely to also play an active role in producing force and movement (Kinosita 1998; Kinosita *et al.* 1998).

In the case of myosin, large-amplitude bending (conformational change) occurs when it binds ATP (Suzuki *et al.* 1998; Dominguez *et al.* 1998), suggesting that the reversal of the bending upon release of the hydrolysis products may directly drive an actin filament. Thermodynamics of actomyosin ATPase (Taylor 1979), however, indicates that much of the free energy of ATP hydrolysis is used in the unbinding of myosin from actin. Thus, rebinding by actin is likely to be the source of the pulling force, at least by reinforcing the reversal of the myosin bending. Whether myosin bound to actin in fact undergoes a large-amplitude bending and, if so, whether the bending produces sufficient force to drive actin, are yet to

be seen. The observation that myosin made several 5-nm steps on actin upon hydrolysis of only one ATP molecule (Kitamura *et al.* 1999) is not readily explained by a simple bending model. Kinesin is likely to 'walk' on a microtubule using its two globular ATPase domains as 'feet'. Even so, whether the force is generated when a 'leg' is bent forward, or when a detached 'foot' is bound to the microtubule, is still an open question. A key to understanding the mechanism of linear motors is to detect their nucleotide-dependent conformational changes while they are bound to the substrate filament, but decisive experiments have not been done.

Two rotary molecular motors are known to date. One is the bacterial flagellar motor that rotates a flagellum using proton flow through the motor as the energy source (DeRosier 1998). The other is the  $F_0F_1$ -ATP synthase (Boyer 1993, 1997, 2000; Junge *et al.* 1997; Kinosita *et al.* 1998, 2000; Kinosita 1999; Kagawa 1999), which comprises two rotary motors, one driven by proton flow ( $F_0$  motor) and the other by ATP hydrolysis ( $F_1$  motor), in one molecule.

The mechanisms of the proton-driven motors, whether flagellar or of ATP synthase, are less clear compared to myosin and kinesin, because structural details have not been elucidated. It is of interest to note that, at least conceptually, these proton-driven motors could operate without major conformational changes in either the rotor or stator: electrostatic force from moving protons could produce torque if the geometry of proton channels are designed appropriately (Lauger 1977).

Large-amplitude bending occurs in the ATP-driven  $F_1$ -motor of the ATP synthase (Abrahams *et al.* 1994). The

\*Author for correspondence.

bending has been shown in a functional motor complex containing both the rotor and stator, and thus this bending is likely to contribute directly to torque generation. Unlike linear motors that undergo alternate binding and unbinding to and from the substrate filaments, the rotor and stator stay together in rotary motors. The analysis of the molecular mechanism of the  $F_1$  motor may, in this sense, be simpler, and is expected to reveal precisely how the energy of ATP hydrolysis can be converted to torque. (Note that, if linear motors produce movement by bending, as in the lever-arm model for myosin, the direct outcome of nucleotide hydrolysis is torque rather than vectorial force.)

## 2. ATP SYNTHASE AND ROTATIONAL CATALYSIS

### (a) *ATP synthase: a reversible molecular machine*

ATP synthase is ubiquitous from bacteria to plants and animals. It is a membrane-spanning enzyme that produces ATP using proton flow across the membrane. In animals, ATP synthase resides in the inner mitochondrial membranes where an electrochemical gradient of protons, high on the outside of mitochondria, is generated by the respiratory chain of enzymes. An active researcher produces his or her bodyweight of ATP in one day.

As shown in figure 1, the ATP synthase consists of a membrane-embedded portion  $F_0$  and a protruding portion  $F_1$ , and thus is also called  $F_0F_1$ -ATP synthase. When protons flow through  $F_0$  from top to bottom, in figure 1, ATP is synthesized in  $F_1$ . The synthase is a completely reversible molecular machine in that, when ATP is hydrolysed in  $F_1$ , protons are pumped back, from bottom to top, against an electrochemical gradient. How, then, is the proton flow through  $F_0$  coupled to the synthesis–hydrolysis of ATP in  $F_1$ ?

### (b) *Boyer's proposal: two rotary motors with a common shaft*

Boyer proposed that the coupling is mechanical (Boyer & Kohlbrenner 1981):  $F_0$  is a motor, or turbine, driven by the proton flow, and  $F_1$  is another motor driven by ATP hydrolysis. The two have a common shaft. Proton flow from top to bottom in figure 1 drives the shaft in a unique direction, say clockwise. ATP hydrolysis in  $F_1$  drives the shaft in the opposite direction, counterclockwise. When the free energy obtained from the downward flow of protons is greater than the free energy of ATP hydrolysis, the  $F_0$  motor rotates the common shaft in its genuine direction. The  $F_1$  motor is forced to rotate in its reverse direction, and thus ATP is synthesized in its catalytic sites. If the energy obtained from ATP hydrolysis is higher, the  $F_1$  motor gains control and protons are pumped out.

Boyer's idea came from the analysis of the chemical reaction in the  $F_1$  part. The  $F_1$  portion can be isolated in solution, and then it only hydrolyses ATP. Hence, the isolated enzyme is called  $F_1$ -ATPase. The  $F_1$ -ATPase consists of five types of subunits in the stoichiometry of  $\alpha_3\beta_3\gamma\delta\epsilon$  (in bovine mitochondrial  $F_1$ ,  $\delta$  and  $\epsilon$  are, respectively, called  $\epsilon$  and OSCP).  $\alpha_3\beta_3\gamma$ -subunits suffice for ATPase activity (and for rotation, as shown in §3(a)). Each  $\beta$ -subunit contributes one catalytic site for the synthesis–hydrolysis of ATP (the catalytic site resides at

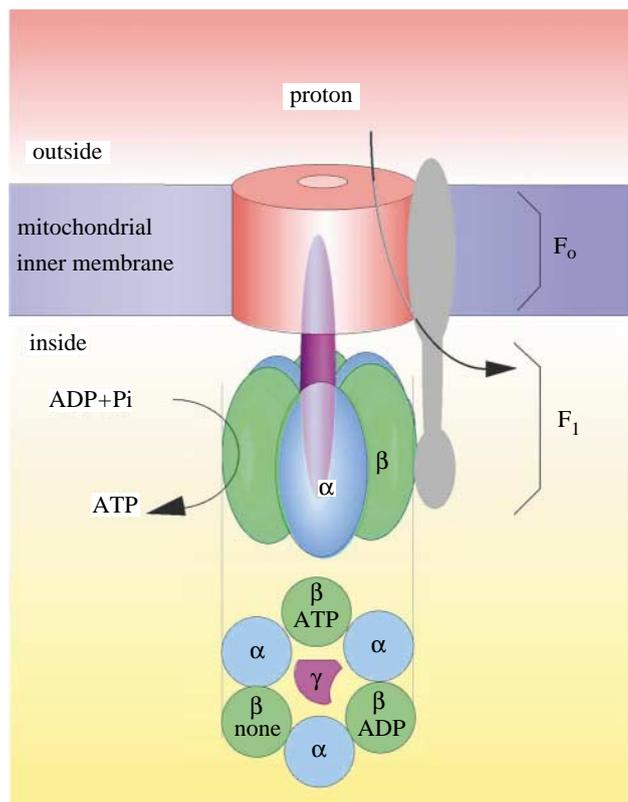


Figure 1. A schematic view of ATP synthase (Kinoshita *et al.* 1998). The magenta rod at the centre represents the common shaft (the  $\gamma$ -subunit). In a currently popular but unproven view, the orange cylinder in the membrane rotates together with the  $\gamma$ -shaft and the grey part serves as the stator. The bottom diagram shows a top view of the  $F_1$  part with catalytic nucleotides as found in the crystal (Abrahams *et al.* 1994).

the interface between a  $\beta$ -subunit and an  $\alpha$ -subunit, and is in part contributed from residues of  $\alpha$ ). In addition, three non-catalytic nucleotide-binding sites exist, one on each  $\alpha$ , but we ignore these non-catalytic sites in most of this review. Now, Boyer and others have found that the three catalytic sites are completely equivalent in steady-state ATP hydrolysis by  $F_1$ -ATPase or in steady-state ATP synthesis–hydrolysis by the whole ATP synthase. The  $\gamma$ -subunit, a single-copy subunit, was known to be indispensable for the catalysis, but its amino-acid sequence indicated that its structure could not possess threefold symmetry. Then, for the asymmetrical  $\gamma$ -subunit to interact with the three  $\beta$ -subunits impartially, it had to rotate. The rotation could be either unidirectional or to-and-fro fluctuation, but there should have been no limit in the rotational angle.

### (c) *Support for the rotational catalysis model*

That a subunit in a compact, functional protein molecule could slide against other subunits over infinite angles was certainly a revolutionary idea. Textbooks teach that protein subunits are held against each other by lock-and-key mechanisms, which would not readily allow mutual sliding. There were few believers, until a three-dimensional structure of  $F_1$ -ATPase was solved by Walker and colleagues (Abrahams *et al.* 1994). In the structure, which we refer to as the 'Walker structure' in this review,  $\alpha_3\beta_3$  hexamer formed an orange-shaped cylinder, and part of

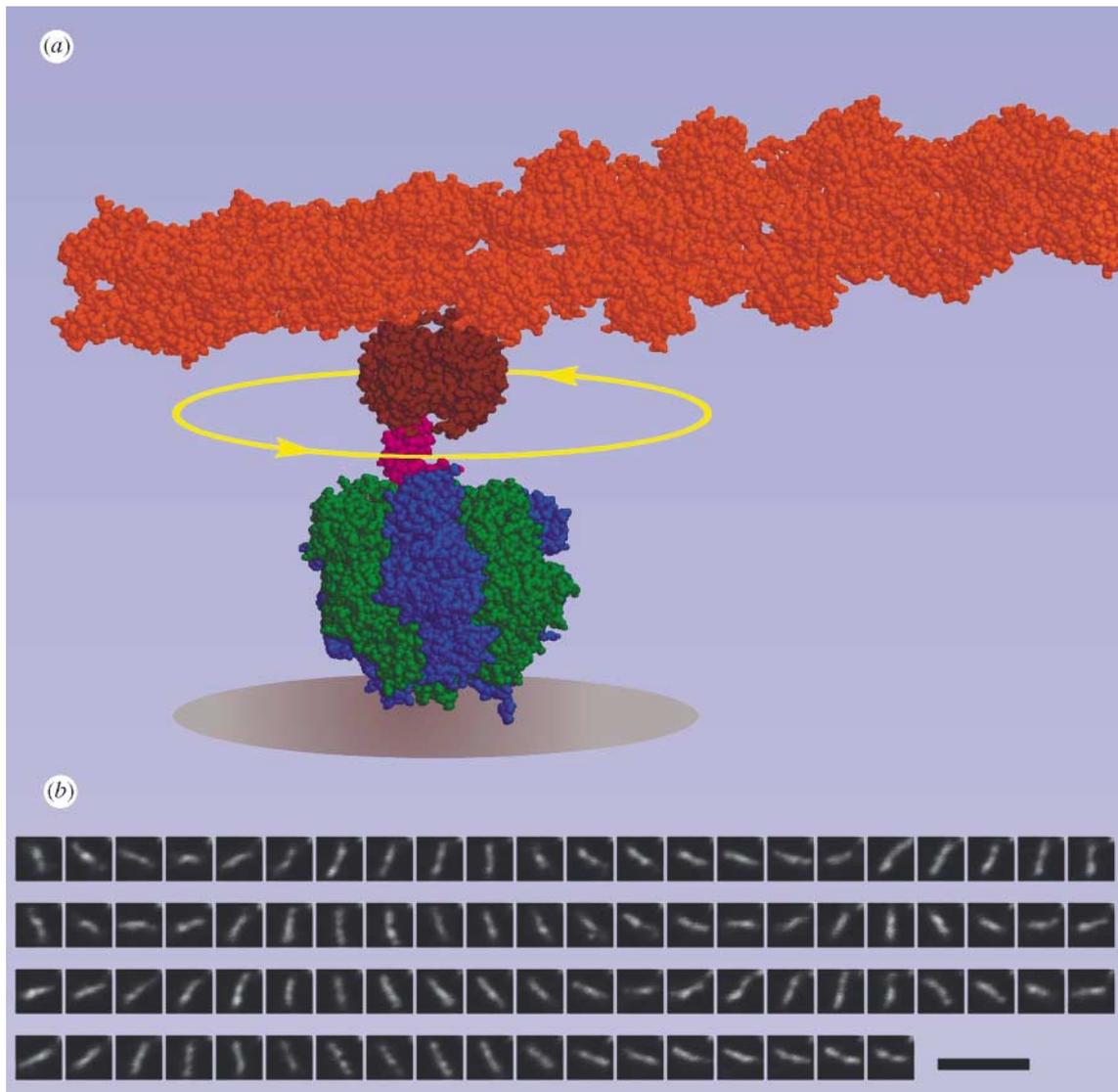


Figure 2. (a) The experimental system for the observation of the rotation of  $F_1$ -ATPase. The space-filling model of  $F_1$  (blue,  $\alpha$ ; green,  $\beta$ ; magenta,  $\gamma$ ) is from Abrahams *et al.* (1994), actin filament (orange) from Holmes *et al.* (1990), and streptavidin (brown) from Livnah *et al.* (1993). Streptavidin has four strong binding sites for biotin, and the actin filament is heavily decorated with biotin. There is, however, only one biotin on  $\gamma$ . Presumably, free rotation between streptavidin and  $\gamma$  is prevented by steric hindrance. The diameter of the grey disk, representing the surface to which the three  $\beta$ -subunits are bound through histidine tags, is *ca.* 22 nm. (b) Sequential images, at 33 ms intervals, of a rotating actin filament (Noji *et al.* 1997). The average rate of rotation was  $1.3 \text{ rev s}^{-1}$ . Bar, 5  $\mu\text{m}$ .

the  $\gamma$ -subunit, in the form of a coiled coil of two  $\alpha$ -helices, penetrated the centre of the cylinder ( $\delta$ - and  $\epsilon$ -subunits were not resolved). The interface between the central  $\gamma$ -subunit and surrounding  $\alpha_3\beta_3$ -subunits was mostly hydrophobic, suggesting that the  $\gamma$ -shaft might rotate in the oily sleeve. Moreover, the three catalytic sites were filled with different nucleotides, one with AMPPNP (an analogue of ATP), the second with ADP, and the third with none, in a clockwise order when viewed from the top of figure 1 (see the bottom of the diagram). If this arrangement represents an active intermediate during hydrolysis, the arrangement in the next hydrolysis step would be ADP, none and ATP. The side of the  $\gamma$ -subunit that tends to face the ATP-carrying  $\beta$ -subunit would thus rotate counterclockwise.

The Walker structure strongly supported Boyer's rotational catalysis model; the  $\gamma$ -subunit would constitute a

part of the common shaft of the two motors. The high-resolution structure immediately suggested experiments that would confirm the rotation of the  $\gamma$ -subunit against the  $\alpha_3\beta_3$  cylinder. One strategy was to cross-link a particular residue on  $\gamma$  to one of the three  $\beta$ s. Then the link was cut and the enzyme was allowed to catalyse ATP hydrolysis ( $F_1$  preparation; Duncan *et al.* 1995) or synthesis (whole ATP synthase; Zhou *et al.* 1997). After that, the residue was again cross-linked to a  $\beta$ -subunit. The second cross-linking was found to be to any of the three  $\beta$ -subunits, indicating that the residue on the  $\gamma$ -subunit faced all three  $\beta$ -subunits equally during catalysis. In experiments where catalysis was not allowed between the two cross-linking treatments, the second target was the same as the first one. In another set of experiments (Sabbert *et al.* 1996; Häsler *et al.* 1998), a fluorescent dye was attached to the  $\gamma$ -subunit. Time-resolved polarization

measurement showed that the fluorophore changed its orientation over many degrees when the enzyme underwent an ATP hydrolysis reaction. In one study (Häsler *et al.* 1998), the fluorophore appeared to adopt three distinct orientations. These experiments together indicated that the  $\gamma$ -subunit indeed rotates in the  $\alpha_3\beta_3$  cylinder, but whether the rotation occurs in a unique direction was unanswered. The answer came from direct imaging of the rotation under a microscope, as described in the next section.

#### (d) *F<sub>0</sub> awaits more experiments*

Relatively little is known about the  $F_0$  motor. A prevailing view for bacterial synthase (Junge *et al.* 1997; Fillingame *et al.* 1998; Oster & Wang 2000) is that 12 c-subunits in the membrane form a cylinder that is attached to  $\gamma$  and together constitute the common shaft. The  $\delta$ -subunit of  $F_1$  and  $ab_2$ -subunits of  $F_0$  together constitute the stator (the grey part in figure 1), which is attached to the  $\alpha_3\beta_3$  hexamer through  $\delta$ . The a-subunit in the membrane apposes the  $c_{12}$  cylinder. Protons flow through the interface between the a-subunit and the  $c_{12}$ -subunits and rotate  $c_{12}$  against a. Recent electron micrographs (Boekema *et al.* 1997; Wilkens & Capaldi 1998) of ATP synthase show a thin, second stalk at a position corresponding to the grey stator in figure 1. One difficulty in this view is that the  $\alpha_3\beta_3$  hexamer should, on time-average, be threefold symmetrical, yet there is one  $\delta b_2 a$  stator attached to it. Also, the  $c_{12}$  cylinder is presumably 12-fold symmetrical, whereas  $\gamma$  needs to be firmly attached to  $c_{12}$  but lacks its symmetry. These may not be serious problems, but certainly detract from the elegance of Boyer's proposal.

### 3. IMAGING $F_1$ ROTATION

#### (a) *A huge tag revealed rotation in a single $F_1$ molecule*

To prove that  $F_1$ -ATPase is a rotary motor that consistently rotates in a unique direction, and to investigate the details of the rotational characteristics, we imaged the rotation of single  $F_1$  molecules under a microscope (Noji *et al.* 1997; Yasuda *et al.* 1998). A subcomplex of  $F_1$ ,  $\alpha_3\beta_3\gamma$  (hereafter we refer to this subcomplex simply as  $F_1$ ) derived from a thermophilic bacterium, was fixed on a glass surface, or on a submicrometre-sized plastic bead sitting on a glass surface, through histidine residues engineered at the bottom of the  $\beta$ -subunits. A micrometre-long actin filament was attached, through biotin-streptavidin links, to the protruding portion of  $\gamma$  above the  $\alpha_3\beta_3$  hexamer (figure 2a). The actin filament was fluorescently labelled, and observed under a fluorescence microscope. When ATP was infused into the observation chamber, the filament began to rotate, as shown in figure 2b.

Only a few per cent of the actin filaments in the observation chamber rotated, but those that rotated did so in the counterclockwise direction, as predicted from the Walker structure. This suggests that a structure similar to the Walker structure, in which rotation was inhibited for crystallization, appears as an active intermediate in the rotational kinetics. Some filaments made hundreds of revolutions without noticeable reversal.

Most of the filaments did not rotate, but there are reasons for this. First, the filaments are likely to stick on the surface, because the height of  $F_1$  is only *ca.* 10 nm, whereas the actin filaments were 1  $\mu$ m or longer. It would be difficult for  $F_1$  to keep the filament level. Indeed, putting  $F_1$  on a 0.2- $\mu$ m bead helped to increase the number of rotating filaments. However, the increase was not dramatic because we could not control the position of  $F_1$  such that it would be precisely at the top of the bead. Second,  $F_1$ -ATPase tends to be inhibited by its reaction product, MgADP (see §4(b)). Third, protein molecules on a surface are often damaged or denatured. In fact, the major job of single-molecule researchers is to find an appropriate surface for the protein of interest, a 'mission impossible' if none of the molecules are to be sacrificed.

In figure 2b, the actin filament rotates around its centre, like a propeller. The propeller rotation shows that the whole  $\gamma$ -subunit slides against the  $\alpha_3\beta_3$  stator over unlimited angles. It is not a fake rotation one could make, for example, by holding an end of a rod over one's head and twisting one's wrist without changing the grip. If one holds the middle of a long rod, one cannot rotate it without occasional releases. Thus, the propeller rotation of the actin filament cannot be made by torsion within the  $\gamma$ -subunit. The  $\gamma$ -subunit has to be separate from the  $\alpha_3\beta_3$  cylinder and truly rotate against the hexamer. Also, the propeller rotation cannot be supported by two or more  $F_1$  molecules. Thus,  $F_1$ -ATPase is a rotary motor made of a single molecule. Its size being *ca.* 10 nm, the  $F_1$ -ATPase is the smallest rotary motor known. Counterclockwise rotation has also been demonstrated for  $F_1$  from *Escherichia coli* (Omote *et al.* 1999; Noji *et al.* 1999) and chloroplast (Hisabori *et al.* 1999).

Of the five kinds of subunit in  $F_1$ ,  $\alpha_3\beta_3\gamma$  suffice for rotation. Cross-linking studies (Aggeler *et al.* 1997) have indicated that  $\epsilon$  is probably a part of the rotor and  $\delta$  belongs to the stator. When an actin filament was bound to  $\epsilon$  instead of  $\gamma$ , the filament also rotated counterclockwise, although the rotary speed was somewhat lower (Kato-Yamada *et al.* 1998).

#### (b) *Stepping rotation*

When ATP concentration was reduced, the rotation became stepwise, as shown in figure 3. The step size of 120° is consistent with, though not a necessary consequence of, the basic threefold symmetry of the  $\alpha_3\beta_3$  stator. We have been unable to resolve sub-steps at the highest temporal resolution, of 5 ms, achieved so far. Note that the motor made a clear back-step at *ca.* 45 s in figure 3. A molecular machine must occasionally make mistakes. The 120° steps have also been confirmed in  $F_1$  without actin (K. Adachi, unpublished data), by attaching a fluorophore on  $\gamma$  and observing the polarization of the fluorescence from the single fluorophore under a microscope (Sase *et al.* 1997; Ha *et al.* 1998). Thus, stepping is not an artefact caused by friction between the actin filament and the stator cylinder with pseudo-threefold symmetry.

### 4. THE KINETICS OF ATP HYDROLYSIS

The hydrolysis kinetics of  $F_1$ -ATPase is complicated, because of the presence of three catalytic sites (and three non-catalytic sites that also bind a nucleotide), and of the

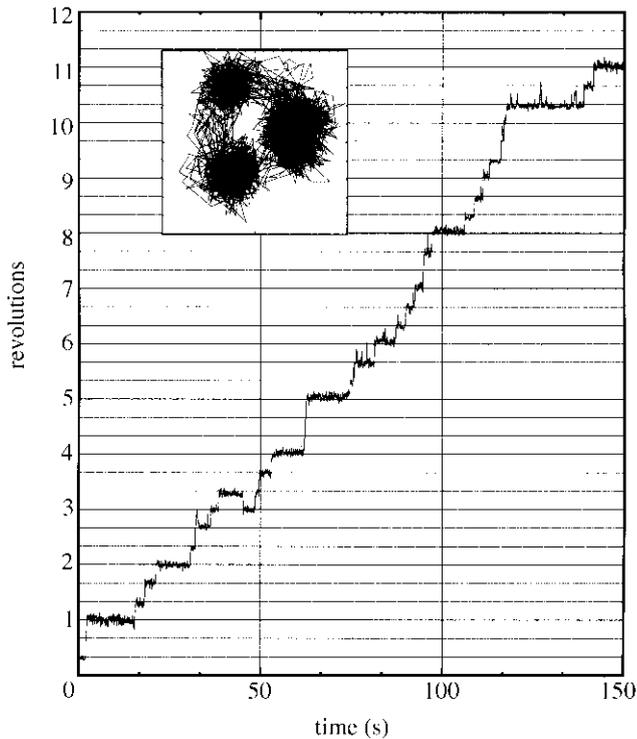
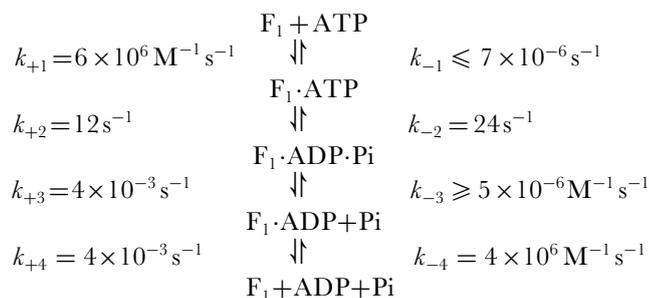


Figure 3. Stepping rotation of  $F_1$  at 20 nM ATP (Yasuda *et al.* 1998). Inset shows the trace of the centroid of the actin filament.

MgADP inhibition. It is difficult to extract a unified view from the literature, partly because the effect of the (almost inevitable) MgADP inhibition on the experimental results is often ignored or not mentioned. The description below is an arbitrary selection from the literature. For comprehensive reviews, see Boyer (1993, 1997, 2000).

#### (a) Three modes of hydrolysis reaction

At extremely low ATP concentrations, at most one catalytic site of  $F_1$  is filled with a nucleotide. Under this uni-site regime, ATP and its hydrolysis products are in equilibrium in the catalytic site, and the products are very slowly released into the medium (figure 4). For mitochondrial  $F_1$ , Cunningham & Cross (1988) describe the uni-site kinetics as



$$\begin{aligned}
 k_{+1}/k_{-1} &= K_1 \geq 10^{12} \text{ M}^{-1}, \\
 k_{+2}/k_{-2} &= K_2 = 80.5, \\
 k_{+3}/k_{-3} &= K_3 \leq 8 \times 10^2 \text{ M}, \\
 k_{+4}/k_{-4} &= K_4 = 10^{-9} \text{ M},
 \end{aligned}$$

where Pi is inorganic phosphate,  $k_{+i}$  and  $k_{-i}$  are forward and backward rate constants, and  $K_i = k_{+i}/k_{-i}$  are the equilibrium constants. Unlike myosin (Taylor 1979), the

rates of ADP and phosphate releases from  $F_1$  appear to be similar, and thus phosphate release does not necessarily precede the release of ADP. A more recent study (Milgrom *et al.* 1998) indicates that the rates of product release ( $k_{+3}$  and  $k_{+4}$ ) are an order of magnitude higher and  $K_2$  is about 0.8. The rate of ATP binding to a second catalytic site (at a higher ATP concentration) is similar to  $k_{+1}$  above (Cross *et al.* 1982). Thus, uni-site catalysis is expected when free ATP concentration is below 1 nM. Uni-site catalysis has been reported to take place even when rotation of  $\gamma$  is prohibited (García & Capaldi 1998). This, however, does not necessarily exclude the possibility that rotation might still accompany uni-site catalysis.

Binding of a second ATP greatly promotes the rate of hydrolysis on the first site and particularly the rates of product release from the first site (Boyer 1993, 1997). The positive cooperativity in catalysis and negative cooperativity in nucleotide binding result in an increase in the overall hydrolysis rate by a factor of more than  $10^3$ . At submicromolar ATP concentrations, hydrolysis occurs in the bi-site mode where, at most, two catalytic sites are filled with a nucleotide (figure 4). Our result in figure 3, the observation of rotation at 20 nM ATP, then indicates that bi-site hydrolysis accompanies rotation.

At higher ATP concentrations, it has often been suggested that hydrolysis proceeds in the tri-site mode with a moderate acceleration from the bi-site mode. One indication has been that the hydrolysis rate over submicromolar to millimolar ATP concentrations, above the uni-site range, cannot be described by simple Michaelis–Menten kinetics (see, for example, dashed line in figure 6) and requires two sets of Michaelis parameters, one presumably corresponding to a second site and the other to the third site. The claim of ‘acceleration’ is based on an approximately tenfold difference in the values of  $V_{\max}$ . Unlike the transition from uni-site to bi-site where doubling ATP concentration more than doubles the hydrolysis rate, however, the acceleration to tri-site is not readily apparent in raw data. The deviation from a simple kinetics is not large (see the example in figure 6), and is variable depending on preparations, possibly due to variability in the degree of MgADP inhibition. Milgrom *et al.* (1998) have reported that, when care was taken to avoid inhibition, one set of parameters ( $K_m = 130 \mu\text{M}$  and  $V_{\max} = 700 \text{ s}^{-1}$  for mitochondrial  $F_1$  at 25 °C) sufficed for the description of the multi-site kinetics up to 1 mM ATP. Thus,  $F_1$ -ATPase may not adopt the tri-site mode. Strong support for tri-site catalysis has come from the measurement of site occupancies through the nucleotide-induced quenching of tryptophans in the catalytic sites (Weber *et al.* 1993). The interpretation of the fluorescence signal, however, is not absolutely unambiguous (Milgrom *et al.* 1998).

Because the rotation of  $\gamma$  has been demonstrated in the bi-site regime, we think that the bi-site mode is fundamental at least for the mechanism of rotation. Bi-site hydrolysis in ATP synthase pumps protons (Muneyuki & Hirata 1988).

#### (b) MgADP inhibition

Figure 5 shows typical time-courses of ATP hydrolysis at three ATP concentrations. The  $\alpha_3\beta_3\gamma$  subcomplex of

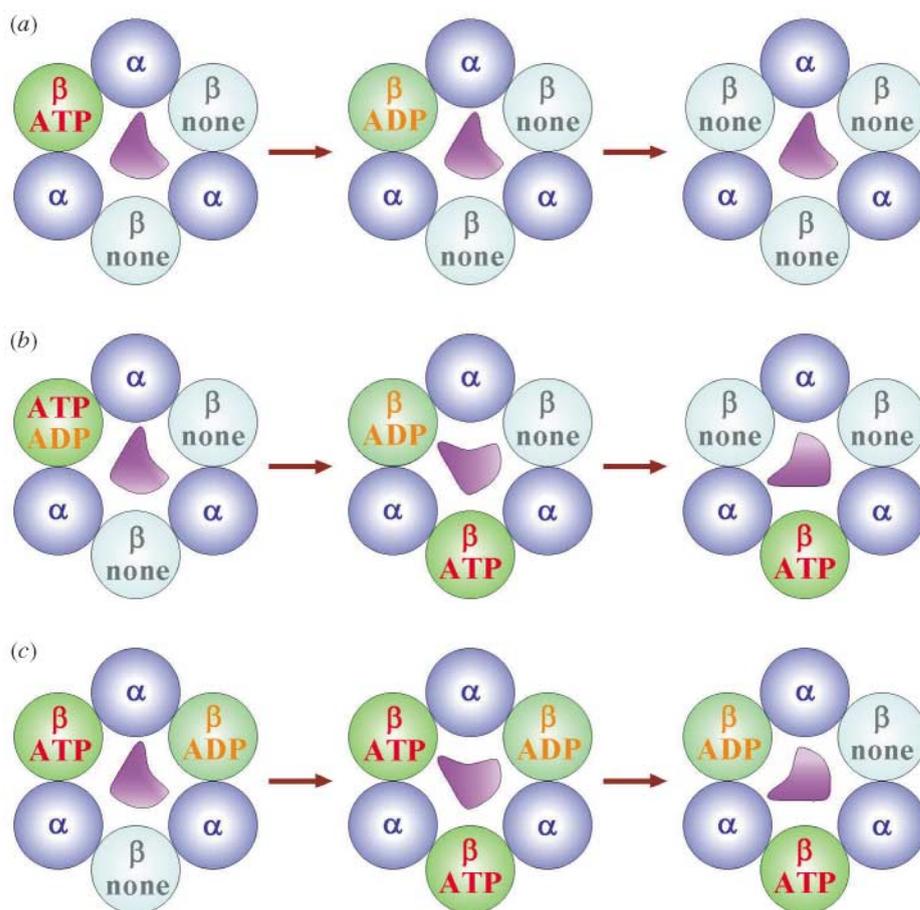


Figure 4. Three modes of ATP hydrolysis by  $F_1$ -ATPase. The timing of  $\gamma$  rotation, and whether  $\gamma$  rotates in the uni-site mode, are yet to be determined. (a) Uni-site hydrolysis,  $[ATP] < 1 \text{ nM}$ ; (b) bi-site hydrolysis,  $[ATP] \text{ ca. } 1 \text{ }\mu\text{M}$ ; (c) tri-site hydrolysis,  $[ATP] > 100 \text{ }\mu\text{M}$ .

bacterial origin used to demonstrate the  $\gamma$  rotation was suspended in solution without attaching actin. The amount of ATP hydrolysed was estimated by regenerating ATP by pyruvate kinase and coupling the reaction to the oxidation of NADH by lactate dehydrogenase (Kato *et al.* 1995). As seen, the rate of hydrolysis gradually decreased to less than half the initial value. This is the so-called MgADP inhibition, where the hydrolysis product MgADP is tightly bound to a catalytic site and inhibits further turnover of the enzyme (Boyer 1997, 2000).

The inhibition does not proceed to completion, because slow binding of ATP to non-catalytic sites tends to displace the tightly bound MgADP in the catalytic site. Under certain conditions, the hydrolysis kinetics becomes tri-phasic: full activity in the initial phase slows down due to the inhibition, and then follows partial recovery toward an intermediate hydrolysis rate (e.g.  $60 \text{ }\mu\text{M}$  in figure 5). In a mutant where ATP binding to the non-catalytic sites was prohibited, there was no recovery and the inhibition proceeded to completion (Matsui *et al.* 1997). In the assay in figure 5, the hydrolysis products were immediately converted back to ATP. If ATPase kinetics is measured without a regeneration system by, for example, chromatographic assay of ATP and ADP, the enzyme is more severely inhibited (E. Muneyuki, personal communication). Thus, a small amount of MgADP in the medium promotes the inhibition.

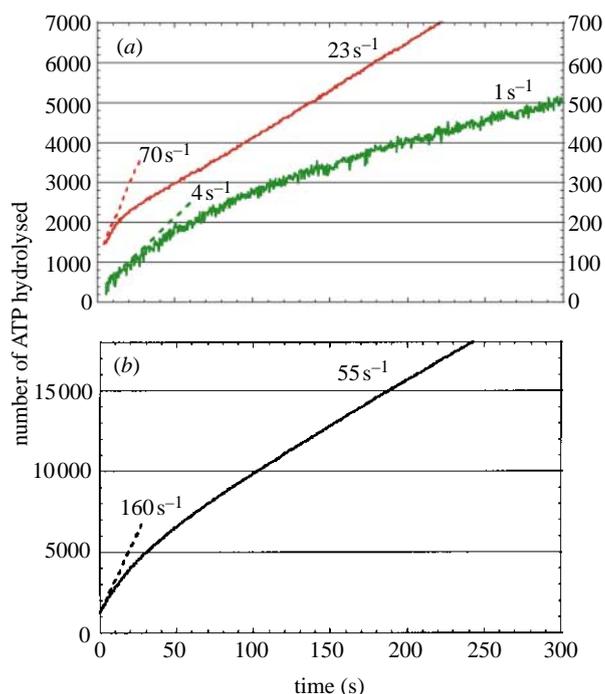


Figure 5. Time-courses of ATP hydrolysis measured in solution at  $23 \text{ }^\circ\text{C}$  (H. Noji, unpublished data). (a)  $[ATP] = 60 \text{ }\mu\text{M}$  shown in red,  $[ATP] = 0.6 \text{ }\mu\text{M}$  shown in green; (b)  $[ATP] = 2 \text{ mM}$ .

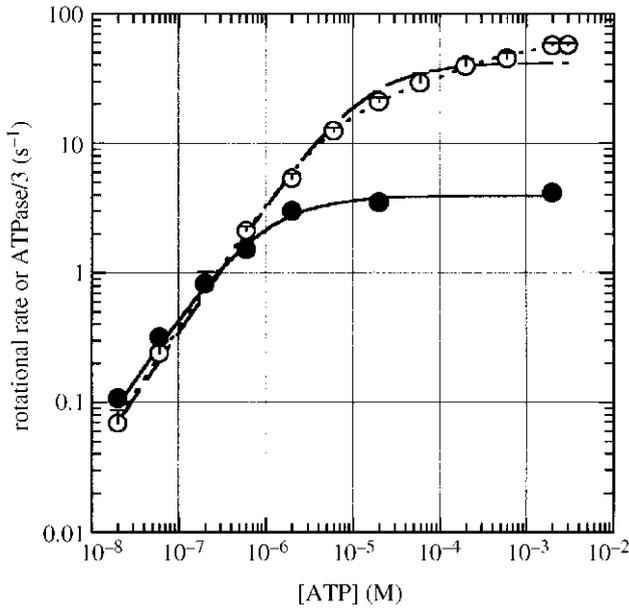


Figure 6. Comparison of the hydrolysis and rotational rates (Yasuda *et al.* 1998). The hydrolysis rate  $V$  (open circles) was measured in solution, and was fitted with  $V = k_{\text{cat}}[\text{ATP}] / ([\text{ATP}] + K_{\text{m}}^{\text{hyd}})$ , where  $k_{\text{cat}} = 125 \text{ s}^{-1}$  and  $K_{\text{m}}^{\text{hyd}} = 12 \text{ }\mu\text{M}$  (dashed line), or with  $V = (k_{\text{cat}}^{\text{a}} K_{\text{m}}^{\text{hydb}} [\text{ATP}] + k_{\text{cat}}^{\text{b}} [\text{ATP}]^2) / ([\text{ATP}]^2 + K_{\text{m}}^{\text{hydb}} [\text{ATP}] + K_{\text{m}}^{\text{hyda}} K_{\text{m}}^{\text{hydb}})$ , where  $k_{\text{cat}}^{\text{a}} = 75 \text{ s}^{-1}$ ,  $k_{\text{cat}}^{\text{b}} = 177 \text{ s}^{-1}$ ,  $K_{\text{m}}^{\text{hyda}} = 6.6 \text{ }\mu\text{M}$ , and  $K_{\text{m}}^{\text{hydb}} = 285 \text{ }\mu\text{M}$  (dotted line). The rotational rate  $v$  was measured by attaching a short (0.8–1.2  $\mu\text{m}$ ) actin filament (closed circles), and was fitted with  $v = v_{\text{max}}[\text{ATP}] / ([\text{ATP}] + K_{\text{m}}^{\text{rot}})$  where  $v_{\text{max}} = 3.9 \text{ rev s}^{-1}$  and  $K_{\text{m}}^{\text{rot}} = 0.8 \text{ }\mu\text{M}$  (solid line).

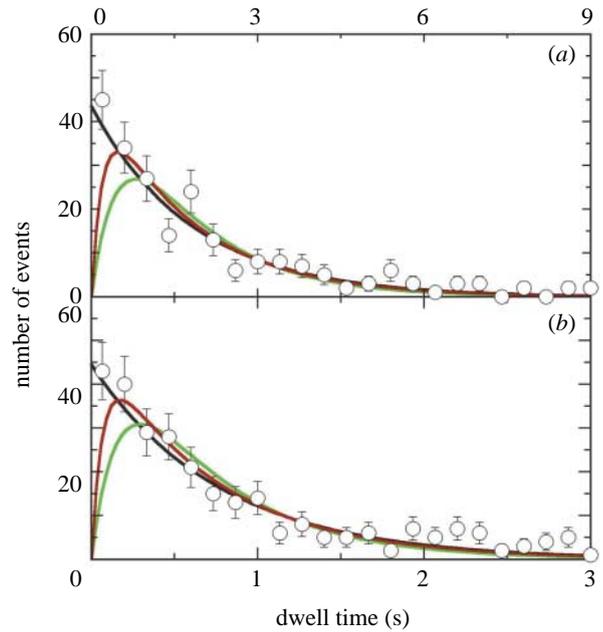


Figure 7. Histograms of dwell times between steps (Yasuda *et al.* 1998). (a)  $[\text{ATP}] = 20 \text{ nM}$ ; (b)  $[\text{ATP}] = 60 \text{ nM}$ . Black lines indicate exponential fits:  $\text{constant} \times \exp(-k_{\text{on}}[\text{ATP}]t)$ , where  $k_{\text{on}}$  is the rate constant for ATP binding ( $2.7 \times 10^7 \text{ M}^{-1} \text{ s}^{-1}$  at 20 nM ATP and  $2.2 \times 10^7 \text{ M}^{-1} \text{ s}^{-1}$  at 60 nM) and  $t$  is the dwell time. Green and red lines show fits with two exponentials (simultaneous consumption of rapidly and slowly bound ATP):  $\text{constant} \times \{\exp(-k_{\text{on}}^{\text{slow}}[\text{ATP}]t) - \exp(-k_{\text{on}}^{\text{rapid}}[\text{ATP}]t)\}$ , where  $k_{\text{on}}^{\text{rapid}}$  was fixed at  $1.0 \times 10^8 \text{ M}^{-1} \text{ s}^{-1}$  (green lines) and  $2.5 \times 10^8 \text{ M}^{-1} \text{ s}^{-1}$  (red lines).

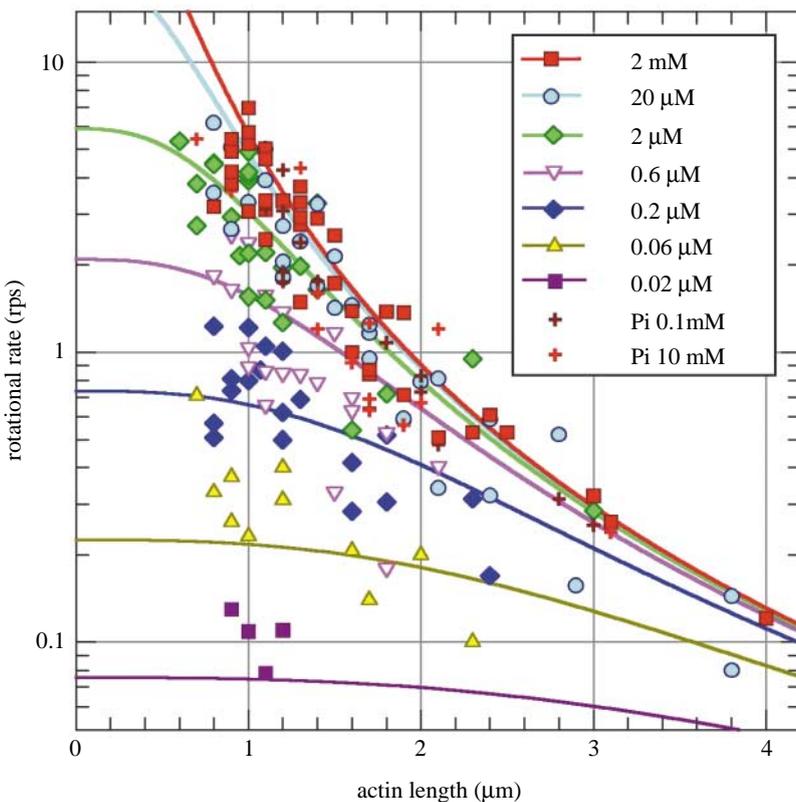


Figure 8. Load (actin length) and ATP dependence of the average velocity of rotation (Yasuda *et al.* 1998). ATP concentrations are shown in the key. ADP and phosphate concentrations were not controlled, except for the + symbols for which  $[\text{ATP}] = 2 \text{ mM}$  and  $[\text{ADP}] = 10 \text{ }\mu\text{M}$ . Lines are calculated as  $1/(3\tau_{120^\circ})$ , where  $\tau_{120^\circ} = \tau_{\text{ATP}} + \tau_{\text{step}}$  is the time per  $120^\circ$  step,  $\tau_{\text{ATP}}$  is the ATP cycle time at no load estimated from figure 6, and  $\tau_{\text{step}} = (2\pi/3)\xi/\mathcal{N}$ , where  $\mathcal{N} = 40 \text{ pN nm}$  and  $\xi$  is the friction coefficient in equation (1). It is likely that  $\tau_{\text{ATP}}$  is overestimated by *ca.* 30% because of the MgADP inhibition, and thus the calculated velocities (lines) at low  $[\text{ATP}]$  are underestimated by the same proportion.

The MgADP inhibition would economize by preventing futile consumption of ATP in cells, but it is a nuisance for researchers analysing the ATPase kinetics. Unless tightly bound nucleotides are completely removed from F<sub>1</sub>-ATPase prior to measurement, which is not often the case, the preparation will contain an unknown amount of inhibited enzyme, possibly most of the molecules. Results on such a preparation, or on the 'steady-state' ATPase, have to be interpreted with caution.

The Walker structure is probably an MgADP-inhibited form (Abrahams *et al.* 1994). As already pointed out, the fact that the arrangement of nucleotides in this structure is consistent with the sense of observed rotation suggests that the Walker structure resembles an active intermediate that appears during rotation. An attempt to 'freeze' F<sub>1</sub>-ATPase in this structure by cross-linking supported this view (Tsunoda *et al.* 1999). Presumably, the inhibited structure represents one of the most stable forms of this enzyme, and is separated by a relatively small activation barrier from the major kinetic pathway of the hydrolysis reaction. In this regard, it is worth noting that MgADP inhibition does not operate during synthesis (Boyer 1997, 2000), and synthesis renders inhibited enzyme back to a form capable of hydrolysis (Galkin & Vinogradov 1999). Free energy obtained by clockwise rotation of  $\gamma$  will lift the enzyme from the bottom of the potential well back to the major pathway, or to a possibly different path for the synthesis.

#### (c) *Three ATP molecules per turn*

The rate of ATP hydrolysis and the rate of  $\gamma$  rotation are compared in figure 6 (Yasuda *et al.* 1998). The hydrolysis rate was measured as the initial rate (figure 5), and is divided by three to facilitate the comparison. The rotational rate was measured with an actin filament of length 0.8–1.2  $\mu\text{m}$ . At ATP concentrations above 1  $\mu\text{M}$ , the rotational rate saturated because of the frictional load imposed on the rotating filament (see §5(a)). Below 1  $\mu\text{M}$  where ATP binding was rate limiting, the rotational rate and one-third of the hydrolysis rate grossly agreed with each other, suggesting that three ATP molecules are consumed per turn.

The agreement was not perfect, a likely cause being the MgADP inhibition. Whereas the rotational rate in figure 6 is the average over selected filaments that rotated vigorously and continuously without unnatural pauses, which represented at most a few per cent of the filaments on the surface, the hydrolysis rate is the ensemble average over all enzyme molecules in the solution. Some molecules in the solution may have been inhibited from the beginning. These samples (also those shown in figure 5) contained about 0.3 M of tightly bound nucleotide per mole of F<sub>1</sub>, implying that 30% may well have been inhibited at the beginning. Also, the initial rate was measured over the first 3–13 s and significant inhibition might have occurred during these periods.

The MgADP inhibition may also be responsible for the failure in fitting the hydrolysis rate with a simple Michaelis–Menten kinetics (solid line in figure 6). Another possible reason is that the non-catalytic sites tend to be filled with ATP earlier at higher ATP concentrations; the hydrolysis rate might be somewhat higher when the non-catalytic sites bind ATP.

#### (d) *One ATP molecule per step*

In figure 6, the rotational and hydrolysis rates are proportional to the ATP concentration in the sub-micromolar range. This suggests that, at least in this range, both processes are fuelled by individual ATP molecules, not by the combination of two or more ATP molecules. To further confirm this point, we analysed the dwell times between rotary steps at very low ATP concentrations where 120° steps were clearly resolved (figure 3).

Figure 7 shows histograms of the dwell times (Yasuda *et al.* 1998). If each 120° step is driven by one ATP molecule, the histogram should be exponential, as was indeed the case (black lines in figure 7). If, on the other hand, two or more ATP molecules were required for each step, the histogram would have started from the origin at the lower left, as in the green and red lines, because simultaneous arrivals of two or more ATP molecules should be a rare event. The data point to one ATP molecule per step. Experimental distinction, however, is not easy when binding of the first ATP molecule is always much faster than the second: in this case the rise of the histogram near the origin will be very steep (compare the green and red lines). As seen, the experimental histograms cannot exclude the two-ATP-molecule case if the rate constant for the first binding is much larger than  $10^8 \text{ M}^{-1} \text{ s}^{-1}$ . Such a high rate (essentially diffusion limited) has not been reported for the hydrolysis kinetics of F<sub>1</sub>-ATPase, whether for uni-, bi-, or tri-site modes.

For the scenario of one ATP molecule per step, the rate constant for ATP binding is estimated from the exponential constant for the histogram:  $2.7 \times 10^7 \text{ M}^{-1} \text{ s}^{-1}$  at 20 nM ATP and  $2.2 \times 10^7 \text{ M}^{-1} \text{ s}^{-1}$  at 60 nM ATP. These values agree, within experimental uncertainty, with each other and also to the slope of hydrolysis rate versus ATP concentration (figure 6). Literature values are scattered mostly between  $10^5$  and  $10^7 \text{ M}^{-1} \text{ s}^{-1}$  (both uni-site and multi-site), and our values here belong to the high end (possibly indicative of the absence of MgADP inhibition).

Judging from figures 6 and 7, we are fairly sure that each 120° step is driven by the hydrolysis of one ATP molecule. Of course this does not necessarily mean that the ATP molecule just bound is hydrolysed and released into the medium during one 120° step: it is highly likely that one ATP molecule is bound to a catalytic site and products are released from a different site, as shown in figure 4. We are less certain about the reverse statement, that each ATP hydrolysis always accompanies rotation. This is suggested by figure 6, but the hydrolysis rate in the complete absence of MgADP inhibition might be somewhat higher than the rotational rate. Futile consumption of ATP, as occurs in the myosin–actin system (Huxley 1957), cannot be ruled out completely.

## 5. MECHANICAL PROPERTIES OF THE F<sub>1</sub> MOTOR

### (a) *The actin filament is a heavy burden for F<sub>1</sub>*

When we observed the rotation of actin filaments attached to  $\gamma$ , we noticed that longer filaments tended to rotate slower. This seemed reasonable, because the hydrodynamic friction against a rotating filament is essentially

proportional to the cube of its length  $L$ : the frictional drag coefficient  $\xi$  is given by (Hunt *et al.* 1994)

$$\xi = (4\pi/3)\eta L^3 / [\ln(L/2r) - 0.447], \quad (1)$$

where  $\eta$  ( $=10^{-3} \text{ N m}^{-2} \text{ s}$ ) is the viscosity of the medium, and  $r$  ( $=5 \text{ nm}$ ) is the radius of the filament. Equation (1) applies to a filament rotating around one of its ends; such filaments were selected for analysis.

The rotational rate  $\omega$  (in radians per second ( $\text{rad s}^{-1}$ )) is related with  $\xi$  and the torque  $\mathcal{N}$  of the motor by

$$\mathcal{N} = \omega \xi. \quad (2)$$

To rotate an actin filament at the observed speed, the  $F_1$  motor has to produce an enormous torque. For example, an actin filament of length  $1 \mu\text{m}$  rotated at  $6 \text{ revs}^{-1}$  ( $\cong 40 \text{ rad s}^{-1}$ ). This requires a torque of about  $40 \text{ pN nm}$ . If this torque is generated at the  $\gamma$ - $\beta$  interface at the radius of  $1 \text{ nm}$ , the force that let  $\gamma$  slide past  $\beta$  amounts to  $40 \text{ pN}$ , the largest among the forces produced by known nucleotide-driven motors (Kinoshita *et al.* 1998).

#### (b) *The $F_1$ motor produces a constant torque*

In figure 8, the rotational rates of actin filaments that made at least five continuous revolutions without unnatural pauses are plotted against the filament length. As seen, the data points at different ATP concentrations, distinguished by different symbols, fall approximately on the respective smooth lines that have been calculated on the assumption of constant torque. That is, we assumed that (i)  $F_1$  produces a constant torque of  $40 \text{ pN nm}$  irrespective of the frictional load (actin length) or of the ATP concentration, and (ii) the time per one-third of a revolution is simply the sum of the ATP cycle time at no load (taken from figure 6) and the time needed to rotate the actin filament by  $120^\circ$  under the torque of  $40 \text{ pN nm}$ . The latter—the time needed to move the filament—was assumed to be given by  $2\pi/3 \text{ rad}$  ( $=120^\circ$ ) divided by  $\omega = \mathcal{N}/\xi$ , where the torque  $\mathcal{N}$  was assumed to be  $40 \text{ pN nm}$  for all curves.

The fair agreement between the data and the curves in figure 8 indicates that the  $F_1$  motor produces a constant torque of  $40 \text{ pN nm}$  over the range of rotational rates between  $0.1$  and  $10 \text{ revs}^{-1}$  and over the range of ATP concentrations between  $20 \text{ nM}$  and  $2 \text{ mM}$ . The slower rate for a longer filament is explained by the higher friction, and the slower rate at a lower ATP concentration is due to the lower rate of ATP binding. The constant torque output of the  $F_1$  motor is contrasted with the force of the myosin-actin motor, which decreases with the sliding speed (Huxley 1957). The bacterial flagellar motor produces a constant torque when the rotary speed is not high (Berg & Turner 1993). In this regard, the rotational rates of the  $F_1$  motor in figure 8 are also low compared to the expected unloaded rate: figure 6 indicates that the maximal rate of ATP hydrolysis in the absence of actin is about  $180 \text{ s}^{-1}$ , implying that the maximal rotational rate will exceed  $60 \text{ revs}^{-1}$  at high ATP concentrations. Indeed, recent measurements show unloaded rotation at *ca.*  $100 \text{ revs}^{-1}$  at  $23^\circ \text{C}$  (R. Yasuda, unpublished data). The torque performance at high rotational rates remains to be determined.

#### (c) *The energy conversion efficiency can be nearly 100%*

The torque of  $40 \text{ pN nm}$  times the angular displacement of  $2\pi/3 \text{ rad}$  ( $=120^\circ$ ), *ca.*  $80 \text{ pN nm}$ , is the mechanical work done in a  $120^\circ$  step. This value of  $80 \text{ pN nm}$  is close to the free energy obtained from the hydrolysis of one ATP molecule under intracellular conditions:  $\Delta G = \Delta G_0 + k_B T \ln[\text{ADP}][\text{Pi}]/[\text{ATP}]$ , where  $\Delta G_0 = -50 \text{ pN nm}$  is the standard free-energy change per molecule for ATP hydrolysis at pH 7,  $k_B T = 4.1 \text{ pN nm}$  is the thermal energy at room temperature, and intracellular  $[\text{ATP}]$  and  $[\text{Pi}]$  are both in the order of  $10^{-3} \text{ M}$ , giving  $\Delta G$  of  $-100 \text{ pN nm}$  for  $[\text{ADP}] = 10 \mu\text{M}$  and  $-90 \text{ pN nm}$  for  $[\text{ADP}] = 100 \mu\text{M}$ . Thus, the  $F_1$  motor appears to work at an efficiency close to 100%.

Most of the observations in figure 8 were made in the presence of the ATP regenerating system, and thus the concentrations of ADP and phosphate were minimal, implying that  $|\Delta G|$  was much larger than  $80 \text{ pN nm}$ . To confirm the high efficiency, therefore, we conducted experiments in the absence of the regenerating system, at  $[\text{ATP}] = 2 \text{ mM}$ ,  $[\text{ADP}] = 10 \mu\text{M}$ , and  $[\text{Pi}]$  at either  $0.1$  or  $10 \text{ mM}$  (crosses in figure 8). Calculated  $\Delta G$  are  $-110 \text{ pN nm}$  for  $[\text{Pi}] = 0.1 \text{ mM}$  and  $-90 \text{ pN nm}$  for  $[\text{Pi}] = 10 \text{ mM}$ . As seen, the rotational rates under these conditions are also on the red line for the torque of  $40 \text{ pN nm}$ , indicating that the work per step is also *ca.*  $80 \text{ pN nm}$ . The  $F_1$  motor is made to produce a constant work per step of *ca.*  $80 \text{ pN nm}$ , and it can work even when the energy supply per step is as low as  $90 \text{ pN nm}$ .

The scatter of data in figure 8 may make the claim of near 100% efficiency dubious. In fact, there were many more actin filaments, not shown in the figure, that rotated with irregular intermissions and thus gave lower average speed. There are, however, many factors that may impede the filament rotation, as already discussed. Another factor that has not been mentioned is that the effective viscosity close to a surface is higher than in the bulk for which equation (1) applies (Hunt *et al.* 1994): for the actin filament close to the surface, the effective viscosity can be three times as high (Noji *et al.* 1997). Of the data points in figure 8, those that are slow may have been affected by these impeding factors. On the other hand, we cannot think of experimental uncertainties that would lead to a gross overestimation of the rotational rate, determined as the average over five or more revolutions. Actin length determined from the fluorescence image is subject to error, but the error is relatively small for a long filament. In some cases, the filament was slightly curved in the image plane, or the rotating end floated from the surface. The curvature or inclination, however, do not affect the interpretation seriously, because they change the effective length as a cosine of the angle; deviation by  $20^\circ$  is noticeable, for which the ratio of the arc length to its chord is  $(\theta/2)/\sin(\theta/2) = 1.01$  (close to 1).

We also analysed the speed of rotation in individual  $120^\circ$  steps observed at low ATP concentrations (Yasuda *et al.* 1998; also see §5(d)). The torque estimated from equation (2) for  $\omega$  measured in each step averaged  $44 \text{ pN nm}$ , and hence the work per step averaged *ca.*  $90 \text{ pN nm}$ , in agreement with the values obtained from the rotational rate averaged over many revolutions.

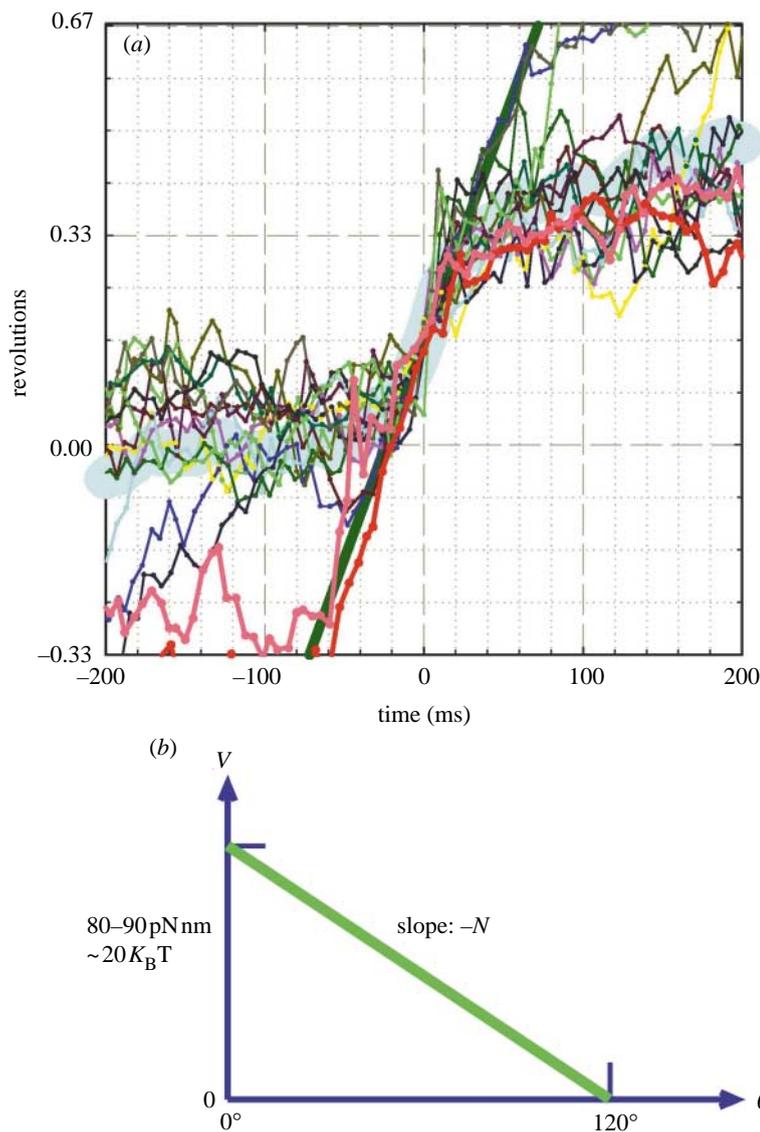


Figure 9. Time-courses of individual steps (Kinoshita *et al.* 2000). (a) Steps were measured at  $0.2 \mu\text{M}$  ATP for  $F_1$  bearing a  $1.0\text{-}\mu\text{m}$  filament. Traces for individual steps are superimposed such that the middle of each step is located at time zero. Rapid succession of two steps are seen in two traces (red and pink). The thick cyan line shows the average of all traces. The thick dark-green line shows a constant-speed rotation at  $44 \text{ rad s}^{-1}$ , corresponding to a torque of  $44 \text{ pN nm}$ . (b) Rotational potential,  $V(\theta)$ , deduced from (a).

Interestingly, the occasional backward steps were as fast as forward steps, implying that the work needed to produce the back step is also *ca.*  $90 \text{ pN nm}$ . Presumably, a backward step also consumes one ATP molecule. In the bi-site catalysis (figure 4), two catalytic sites remain empty for most of the time. Binding of ATP to the wrong one of the two may well cause the backward step. Or, the back step may result from premature dissociation of newly bound ATP before hydrolysis.

**(d) The torque is constant over the rotational angle**

In figure 9a, individual steps for a  $1\text{-}\mu\text{m}$  filament rotating at  $0.2 \mu\text{M}$  ATP are superimposed on each other. As seen in the thick cyan line showing the average, the steps were made at an approximately constant speed from beginning to end. The linearity is clearer in the two curves (red and pink) showing succession of two steps starting at  $-0.33$  revolutions.

The constant speed implies, according to equation (2), a constant torque over the stepping angle of  $120^\circ$ . The thick green line indicates that the constant torque is about  $44 \text{ pN nm}$ . If this torque  $\mathcal{N}$  ( $=44 \text{ pN nm}$ ) is

derived from an angle-dependent potential energy  $V(\theta)$ :

$$\partial V / \partial \theta = -\mathcal{N}, \quad (3)$$

then the potential will be linearly downhill as shown in figure 9b. The depth of the potential is given by  $\mathcal{N}$  ( $=44 \text{ pN nm}$ ) multiplied by  $2\pi/3$ , or *ca.*  $90 \text{ pN nm}$ , in accordance with the work per step of  $80\text{--}90 \text{ pN nm}$  above. The fact that the  $F_1$  motor produces a constant torque and constant work per step irrespective of the load, speed, and ATP concentration, is easily understood if ATP binding and subsequent hydrolysis somehow produces the rotational potential depicted in figure 9b.

Note that the chemical state of bound nucleotides probably changes while the motor makes a  $120^\circ$  step, and thus the potential in figure 9b does not necessarily correspond to a single chemical state. There may well be several chemical states during one mechanical step, each with a different potential. The experimental potential described here (figure 9b) should be regarded as an effective potential.

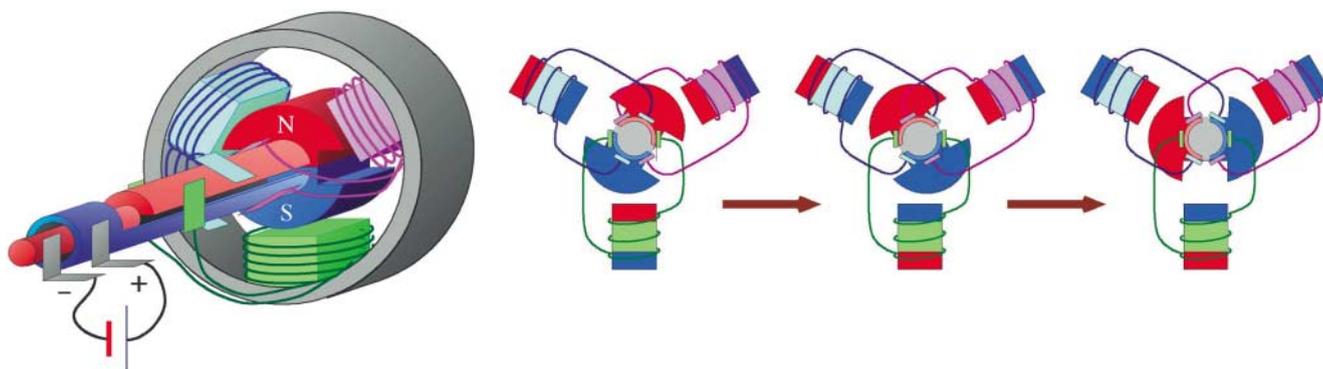


Figure 10. A three-pole DC motor (Kinosita *et al.* 2000). The commutators on the shaft control the polarity of stator magnets such that the shaft rotate continuously counterclockwise.

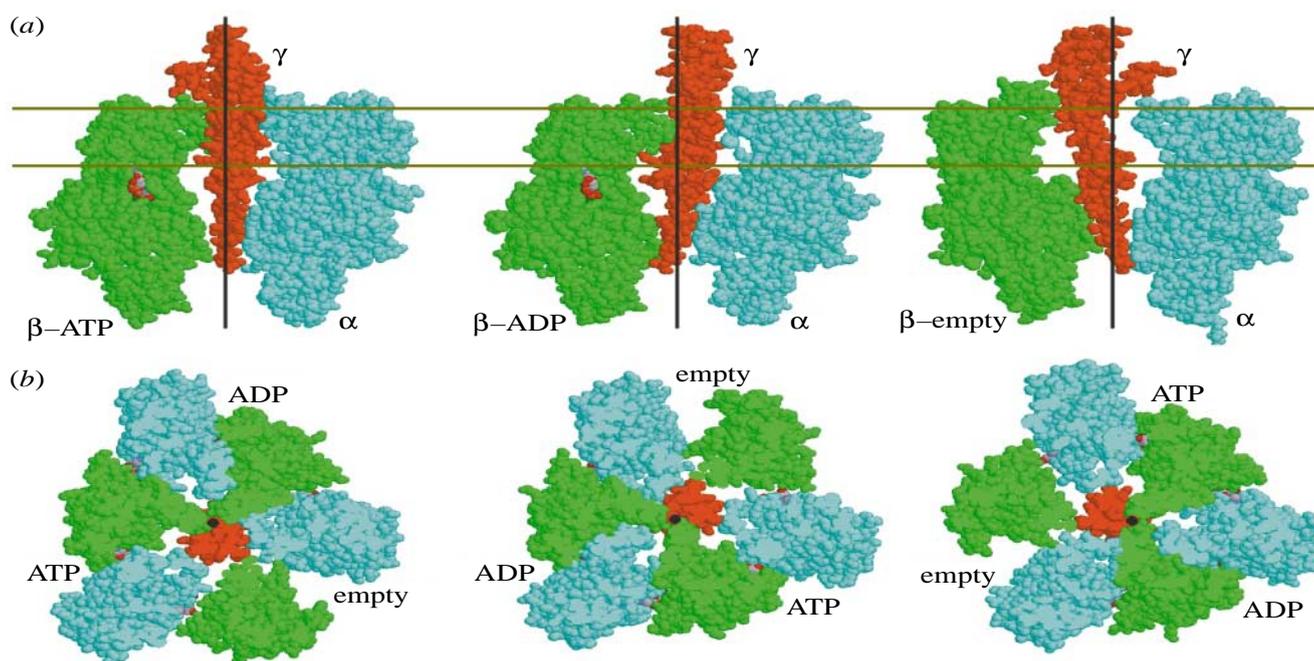


Figure 11. Nucleotide-dependent conformational changes in  $F_1$  (Kinosita *et al.* 2000). (a) From the crystal structure (Abrahams *et al.* 1994), the central  $\gamma$ , one  $\beta$  to the left of  $\gamma$ , and one  $\alpha$  to the right are selected and shown. The black lines indicate the rotation axis suggested by Wang & Oster (1998): the lower half of  $F_1$  retains an approximate threefold symmetry around this axis. Nucleotides are shown in CPK colours. (b) Top view of sections of  $F_1$  between the gold lines in (a).

The torque of 44 pN nm in figure 9a is the torque under the bi-site condition (submicromolar ATP). A similar torque value of 40 pN nm is deduced at 2 mM ATP (figure 8), which is in the putative tri-site regime. Thus, tri-site operation, if it occurs, does not add power to this motor.

## 6. POSSIBLE MECHANISMS OF ROTATION

### (a) Probable experimental facts about the $F_1$ motor

Before discussing the mechanism, we summarize below probable facts about the  $F_1$  motor. We say probable because, in general, there are few experiments from which one can draw conclusions with certainty.

- (i)  $F_1$ -ATPase is a rotary motor made of a single molecule. The energy source is ATP.
- (ii)  $\alpha_3\beta_3\gamma$  suffice for rotation and ATP hydrolysis.  $\gamma$  is the rotor and  $\alpha_3\beta_3$  hexamer is the stator.

- (iii) The rotation of  $\gamma$  is counterclockwise when viewed from the  $F_0$  side.
- (iv) The motor rotates in discrete  $120^\circ$  steps, at least at low ATP concentrations.
- (v) The  $F_1$  motor is so designed as to produce a constant torque of *ca.* 40 pN nm over broad ranges of speed and load, and of ATP concentration.
- (vi) The mechanical work done in each  $120^\circ$  step is also constant, except for statistical variations, and amounts to 80–90 pN nm.
- (vii) Hydrolysis of one ATP molecule suffices for making one step.
- (viii) The energy conversion efficiency approaches 100% when the free energy of ATP hydrolysis is decreased to the intracellular level.
- (ix) Bi-site catalysis supports rotation. The torque in the bi-site regime is as high as the torque in the putative tri-site regime at high ATP concentrations.

- (x) Apparently, each step is made along a linear, downhill potential with a depth of 80–90 pN nm.
- (xi) Back steps occur occasionally.

### (b) *Analogy might help*

A mechanism that is guaranteed to rotate is shown in figure 10. This direct current (DC) motor has three driving poles in the stator part, like the  $F_1$  motor. The motor is powered by a unidirectional current, while ATP hydrolysis is also practically unidirectional. Continuous, counterclockwise rotation of the DC motor is assured by the three pairs of switches on the shaft (commutators), which alternate the polarities of the stator magnets. The rotor is made of a static magnet. The DC motor operates in the bi-site mode in that the three stator magnets never adopt the same polarity at the same time. The DC motor becomes a DC generator if the rotor shaft is forcibly rotated in the clockwise direction. The energy-conversion efficiency of modern electrical motors is quite high, often >95%. Thus, there are apparent similarities between this three-pole DC motor and the  $F_1$  motor. There might be similarities in their operational principles, too.

The driving forces in the DC motor in figure 10 are the attraction between north and south poles and the repulsion between like poles. Wang & Oster (1998) suggest that such a push–pull mechanism may also operate between the  $\gamma$ - and  $\beta$ -subunits of the  $F_1$  motor. Figure 11*a* shows side views of the three pairs of opposing  $\beta$ - and  $\alpha$ -subunits, together with the central  $\gamma$ , in the Walker structure. The vertical black lines show the rotational axis suggested by these authors: the bottom part of the  $\alpha_3\beta_3$  stator has an approximate threefold symmetry around this axis, and thus the conformations of  $\beta$  and  $\alpha$  in the bottom do not change greatly depending on the bound nucleotide. In contrast, in the upper part the  $\beta$ s binding ATP or ADP are bent towards, and therefore push,  $\gamma$ , whereas the empty  $\beta$  retracts and pulls  $\gamma$  towards it. Wang & Oster (1998) suggest that, because the central  $\gamma$  is slightly bent and skewed, cooperative push–pull actions of the three  $\beta$ s would rotate  $\gamma$  as seen in figure 11*b*.

### (c) *An $F_1$ model relying on switches*

Figure 12 shows a model for  $F_1$  rotation based on the push–pull mechanism above, a simplified version of the model proposed by Wang & Oster (1998). The side of  $\gamma$  that faces the empty  $\beta$  in the Walker structure is designated the north pole (N), and thus an empty  $\beta$  is the south pole (S). A nucleotide-carrying  $\beta$  is N, and repels the N face of  $\gamma$  and attracts its S face. By reciprocity, the S face of  $\gamma$  augments the affinity of opposing  $\beta$  for a nucleotide, and the N face decreases the affinity (the free energy is lowered when N and S oppose each other). To make this model rotate in a unique direction, additional control of nucleotide binding kinetics via ‘commutators’ is required. A simple example is given in figure 12*b*: binding–release of ATP is allowed for  $\beta$  while it is on the pink side of  $\gamma$ , and ADP binding–release while on the green side. As shown in figure 12*c,d*, the switching ensures counterclockwise rotation of  $\gamma$  when ATP is hydrolysed; when the rotor is forced to rotate clockwise in the presence of ADP (and phosphate), ATP is synthesized. (We do not distinguish ADP, ADP plus phosphate, or

phosphate alone, because the rate constants for ADP and phosphate releases are similar and because we do not yet know which event is pivotal in producing rotation.)

More elaborate switches have been proposed by Wang & Oster (1998; also see Oster & Wang 2000), and their model can account for many experimental observations including the near 100% efficiency and 120° stepping with occasional back steps. In their model, as with the model in figure 12, the motor tends to pause at angles of 60° out of phase from the Walker structure (figure 12*a*), a prediction experimentally testable. How the switching action is implemented in the protein structure is yet to be specified.

### (d) *A switch-less $F_1$ model*

The roles of the commutators in figure 10 are to alternate the polarities of the stator magnets, and to do so at precise timings dictated by the rotational angle of the shaft. Unlike the magnet driven by direct current, the alternation of the polarity is inherent in the ATP-driven ‘magnet,’ where bound ATP is eventually hydrolysed and released, and the S state is restored spontaneously. Thus, only coordination of nucleotide kinetics among the three stator magnets needs be programmed. This could be done without postulating switches, as shown in figure 13, which is one version of the general model of Oosawa & Hayashi (1986).

In figure 13, the position of the ‘magnetic pole’ in  $\beta$  changes depending on the bound nucleotide. This dual-pole arrangement, combined with the higher affinity for nucleotides when the pole is closer to the S face of  $\gamma$ , ensures counterclockwise rotation in bi-site hydrolysis by inducing ATP binding primarily in the empty  $\beta$  in the counterclockwise direction (figure 13*c*). Note that the angle dependence of the nucleotide affinity is a result of the reaction to nucleotide-dependent push–pull action, and that this angle dependence does not require switches. An additional factor warranting correct rotation in this model is the higher affinity for ATP than for ADP. Because ATP hydrolysis on  $\beta$  is reversible (the free-energy difference between  $\beta$  binding ATP and  $\beta$  binding ADP + phosphate is small), the affinity for the hydrolysis products has to be lower in order for  $\beta$  to act as ATPase. In the original model of Oosawa & Hayashi (1986), near 100% efficiency was achieved for both hydrolysis and synthesis.

The essence of the dual-pole arrangement is that the hydrolysis of ATP to ADP on a  $\beta$ -subunit produces rotational force, and the release of ADP tends to further rotate  $\gamma$ . That is, direct rotational force, in addition to the pushing–pulling, is produced by a single  $\beta$  hydrolysing ATP. Apparently, the Walker structure gives more emphasis to pushing–pulling than direct rotation, but the structure of  $\gamma$  in the protruding portion has not been resolved. Also, a key intermediate(s) in actual rotation, particularly the state with only one bound nucleotide among the catalytic sites, may well have a somewhat different structure. Boyer (1997, 2000) points out that the equilibrium between ATP and its hydrolysis products on  $\beta$  is shifted depending on whether ATP synthase is synthesizing or hydrolysing ATP. The switch-less model predicts this behaviour because clockwise rotation of  $\gamma$  shifts the equilibrium towards ATP and counterclockwise rotation towards ADP (figure 13*c,d*).

The abstract models in figures 12 and 13 might help dissect the actual  $F_1$  motor, but they are nothing more than a guide. The magnetic representation obscures several factors that may be important. For example, unlike the magnets, actual  $\gamma$  and  $\beta$  do not possess reflection symmetry. The force between  $\gamma$  and individual  $\beta$  must therefore be more or less asymmetrical, favouring one rotational direction over the other, as modelled by the dual poles in figure 13. Whether the rotational potential can be approximated by a simple superposition of three pairwise interactions between individual  $\beta$  and  $\gamma$ , as implied by the magnetic representation, may also be questioned. In figures 12 and 13, nucleotide kinetics on different  $\beta$ s are coordinated only through the rotation of  $\gamma$ , but  $\beta$ s may also communicate with each other through intervening  $\alpha$ s.

## 7. PROSPECTS

### (a) $F_1$

When do we say we have understood the mechanism of  $F_1$  rotation, or of molecular motors in general? The  $F_1$ -ATPase has given us the unique opportunity of determining the mechanical potential that underlies the force and movement. The potential in figure 9*b*, however, is an apparent one, and we do not yet know how it is formed, except for guess work. We need to, and should be able to, determine the mechanical potential for each chemical state of the bound nucleotides. The chemical state, at least which of the binding sites are filled with a nucleotide, could be measured with single-molecule imaging of fluorescent nucleotides (Funatsu *et al.* 1995) or by introducing a probe fluorophore within the binding site (Weber *et al.* 1993). The potential could be estimated by forcibly rotating the  $\gamma$ -subunit, for example with optical tweezers. As we discussed above, the potential and the affinity for nucleotides are in a sense mirror images of each other: if, for example, ATP binding favours a certain orientation of  $\gamma$ , that orientation increases the affinity for ATP. Thus, measurement of nucleotide affinity also serves as an indirect means of estimating the potential.

When we know the potentials for individual chemical states involved in rotation, we would like to ask how each of them is formed. We wish to answer on the basis of the atomic structure of the  $F_1$  motor. Here, the vitally important structure is yet to be solved: the structure in which only one catalytic site is filled with a nucleotide, the structure from which the bi-site stepping begins. Presumably, the transition from this structure to something similar to the Walker structure drives the rotation. The key issues are whether the two empty  $\beta$ s in the one-nucleotide structure adopt the conformation of the empty  $\beta$  in the Walker structure, and if not, whether the  $\beta$  with a different structure may contribute to the production of a rotational force, perpendicular to the push-pull direction in figure 11. If the force along the direction of rotation is absent, switches are required, and their physical construct should be explored.

The structure of  $\alpha_3\beta_3$  hexamer without  $\gamma$  and without nucleotides has been solved (Shirakihara *et al.* 1997); all three  $\beta$ -subunits adopted a conformation closely resembling the empty  $\beta$  in the Walker structure. The hexamer without  $\gamma$  is not stable in the presence of nucleotides. In

contrast,  $F_1$ -ATPase or the  $\alpha_3\beta_3\gamma$  subcomplex are not stable in the absence of nucleotides (except for those from thermophilic bacteria, which are relatively stable). The  $\gamma$ -subunit appears to favour at least two  $\beta$ s to be in the nucleotide-binding conformation.  $F_1$  bearing only one catalytic nucleotide is probably less stable, and thus shows a high affinity for a second nucleotide. Binding of ATP to the second site thus releases free energy that can be used for rotation. Because the one-nucleotide structure is probably less stable, its crystallization may not be easy. Determination of the structure may require indirect means such as the fluorescence energy transfer technique. A recent cross-linking study has suggested that the one-nucleotide structure is different from the Walker structure (Tsunoda *et al.* 1999).

Experimental determination of mechanical potential is feasible in the case of  $F_1$ , but is not easy for linear motors such as myosin and kinesin that undergo attachment-detachment cycles. These latter motors may use biased Brownian motion and selective binding as a source of movement and force, in addition to potential-driven bending (Huxley 1957; Kinosita *et al.* 1998). Such a thermal ratchet mechanism should be explored in linear motors, not in  $F_1$  for which efficiency appears to be too high for a thermal ratchet to be operative.

The  $F_1$  motor also offers an opportunity of demonstrating conversion of mechanical energy into chemical energy: mechanical synthesis of ATP by forced, clockwise rotation of  $\gamma$ . Nowadays most people believe  $F_1$  in intact ATP synthase will do this, but experimental proof with isolated  $F_1$  is awaited.

### (b) $F_0$

Recently, two crystal structures have been reported that elucidate the link between  $\gamma$  and  $F_0$ . In a crystal of yeast  $F_0F_1$  (Stock *et al.* 1999), a ring of ten (not 12) c-subunits was connected to  $\gamma$  and  $\epsilon$  ( $\delta$  in yeast nomenclature), as shown in figure 14*a,b* (part of the densities assigned to  $\gamma$  are not shown in this figure). Much of the  $\gamma$ -subunit was revealed (figure 14*c,d*) in a crystal of  $F_1$  from *Escherichia coli* (Hausrath *et al.* 1999). Despite the differences in crystal forms, the structures of  $\gamma$  in the two crystals appear largely similar to each other. In particular, contact between  $\gamma$  and the c-ring is indicated in the yeast structure, near the putative rotation axis (black dot and line in figure 14*a,b*). The top of  $\gamma$  in figure 14*c,d* coincides with the contact region.

The structure in figure 14*b* suggests that, when the  $\alpha_3\beta_3$  hexamer is fixed on a surface and ATP is supplied, the c-ring and  $\epsilon$  will rotate together with  $\gamma$ . Indeed, an actin filament attached to  $\epsilon$  in  $F_1$  preparation (Kato-Yamada *et al.* 1998) or c in  $F_0F_1$  preparation (Sambongi *et al.* 1999) was seen to rotate. Whether the c-ring (and  $\epsilon$ ) in intact ATP synthase is a rotor and rotates against its putative stator (the grey part in figure 1), however, remains to be seen. The presence of an intact stator was assumed in the  $F_0F_1$  experiment (Sambongi *et al.* 1999), but the stator did not impede the rotation at all, and the rotation was poorly inhibited by an  $F_0$  inhibitor. In this regard, it is of interest to note that the yeast crystal contained only  $F_1$ -subunits and c, although the 'mother' solution contained a full complement of  $F_0F_1$  (Stock *et al.* 1999). The putative stator appears to be quite labile in the presence of

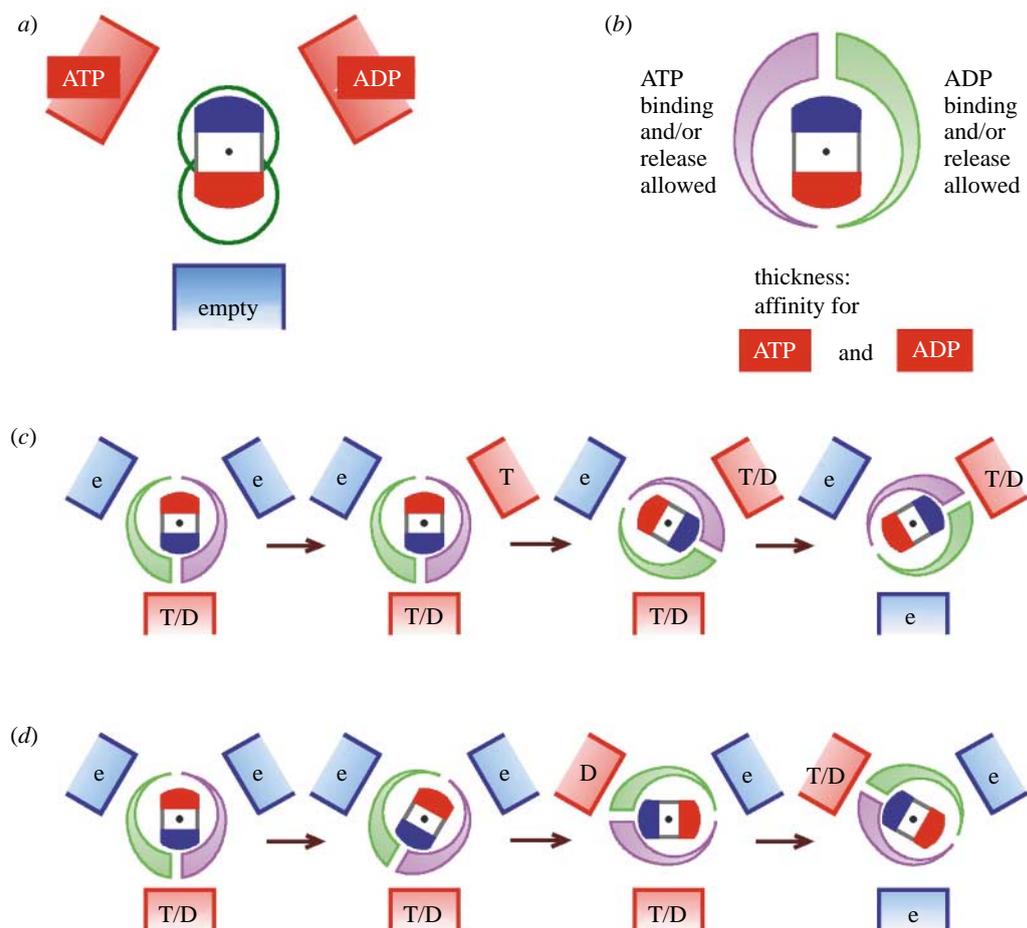


Figure 12. A simple model for the F<sub>1</sub> motor (Kinoshita *et al.* 2000). (a) The Walker structure. The  $\gamma$ -subunit is regarded as a permanent magnet, the side of  $\gamma$  that faces the empty  $\beta$  in the Walker structure being the north pole. (b) The affinity for a nucleotide is higher when  $\beta$  is closer to the south pole of  $\gamma$  (strictly, the affinity for ATP is higher than that for ADP). Binding and release of ATP and ADP are kinetically inhibited on the right- and left-hand sides, respectively. (c) Bi-site hydrolysis ([ATP] > 0, [ADP] *ca.* 0). Bound ATP (T) is in equilibrium with ADP (D) and phosphate, and is released as ADP when a second ATP binds and rotates  $\gamma$ . (d) Bi-site synthesis ([ATP] *ca.* 0, [ADP] > 0). Forced, clockwise rotation of  $\gamma$  results in the uptake of ADP (and phosphate) and release of ATP.

detergent, an indispensable component for the purification of F<sub>0</sub> or F<sub>0</sub>F<sub>1</sub>.

The arrangement of the c-ring in figure 14*a,b* apparently poses a problem. The ring is inclined against the putative rotation axis, and the attachment to  $\gamma$  is not at the centre of the ring. When  $\gamma$  rotates, the ring will make an eccentric movement. The putative stator, while moving the ring to rotate  $\gamma$ , has to maintain close contact with this eccentric ring by bending itself and/or  $\gamma$ . A proton channel(s) must also be secured. A hand-over-hand mechanism, like kinesin, may solve this dilemma, possibly by coordinating structural changes (Rastogi & Girvin 1999) in two or three c-subunits, such that at least one c-subunit is tightly bound to the stator. Occasionally, though, the grip may fail and the c-ring may swing away. Is it then ATP hydrolysis that brings the ring back to the stator surface?

If there were three stators, the c-ring would not escape, and the symmetry mismatch with the  $\alpha_3\beta_3$  hexamer would also be solved. The symmetry mismatch between the three stators and ten c-subunits would be advanta-

geous for c rotation. Two peripheral stalks, in addition to the central  $\gamma$ , have been seen in an electron micrograph of V-type ATPase, raising the possibility of three peripheral stalks at least for this enzyme (Boekema *et al.* 1999). Is it not possible that F<sub>0</sub>F<sub>1</sub> is stripped of some stator components during detergent purification?

It is possible that, in intact synthase,  $\gamma$  is connected to the centre of the c-ring. A central contact with the symmetrical ring, however, would be more liable to slippage than the peripheral contact in figure 14*a,b*. Note that the c-ring might be neither a rotor nor a stator: it could rotate  $\gamma$  by a circular or conical movement without changing its orientation, like a sleeve on a crank handle.

Assignment of rotor subunits apart, the real challenge is to demonstrate, and to elucidate the mechanism of, rotation driven by proton flow. Kaim & Dimroth (1999) have shown that proton gradient alone is not sufficient for ATP synthesis and that transmembrane potential is required. We therefore like to design an experiment in which individual F<sub>0</sub>F<sub>1</sub> molecules are observed while they are exposed to an electric field.

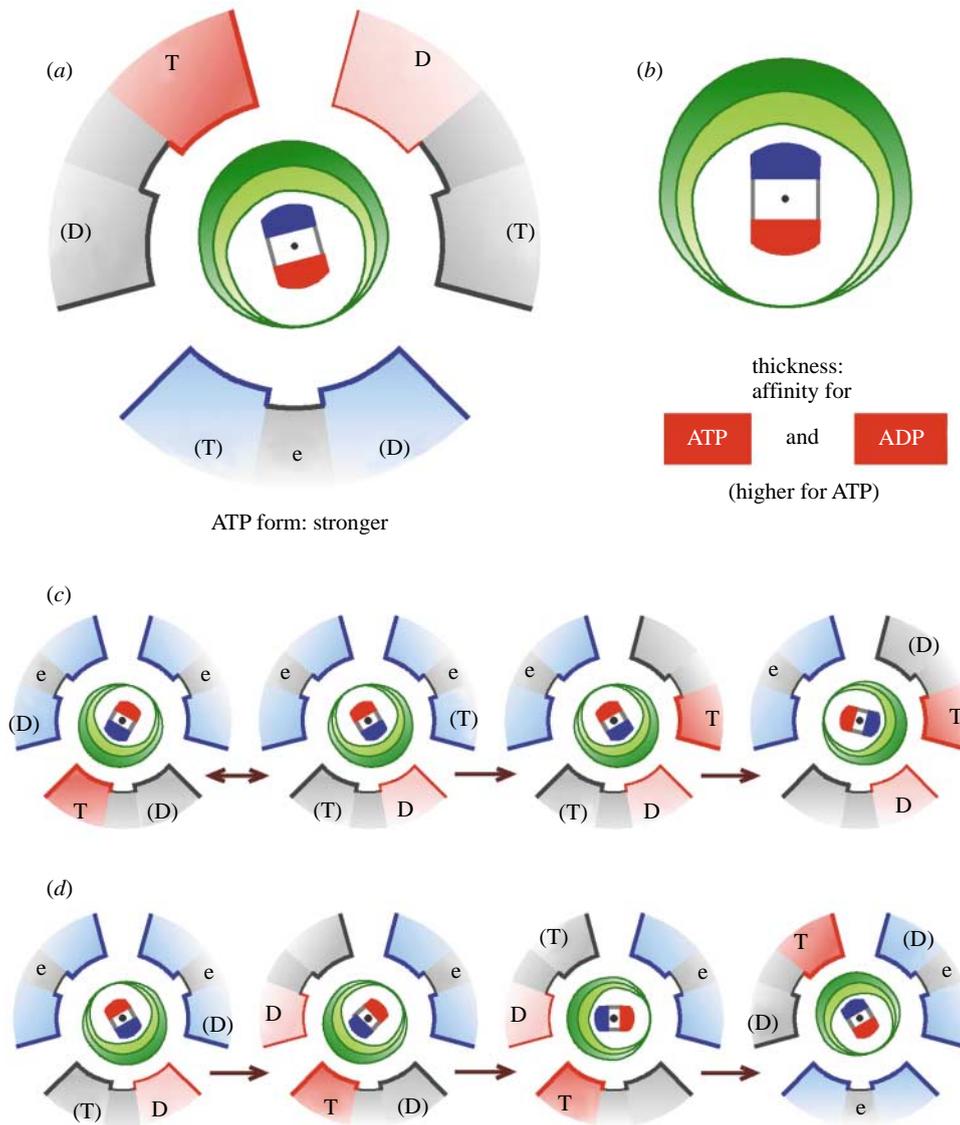


Figure 13. A switch-less model for the  $F_1$  motor (Kinosita *et al.* 2000). (a) The Walker structure. Location of the magnetic pole on  $\beta$  changes depending on the bound nucleotide. ATP magnet is stronger than ADP magnet, and hence, (b) the affinity for ATP is higher than that for ADP (no switches on  $\gamma$ ). (c) Bi-site hydrolysis ([ATP] > 0, [ADP] *ca.* 0). When only one nucleotide is bound, it is reversibly converted between ATP and ADP-phosphate. Comparison of affinities suggests that the most likely way of filling a second site is binding of ATP in the  $\beta$  in the counterclockwise direction. (d) Bi-site synthesis ([ATP] *ca.* 0, [ADP] > 0). When  $\gamma$  is forcibly rotated clockwise, the equilibrium between ATP and ADP is shifted towards ATP, which is eventually released while ADP is newly bound in the second site.

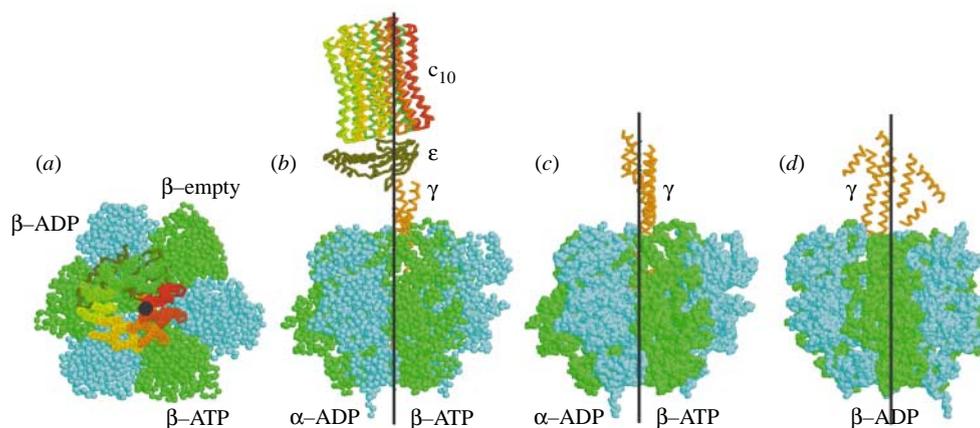


Figure 14. Crystal structures of yeast  $F_0F_1$  (Stock *et al.* 1999) and of *Escherichia coli*  $F_1$  (Hausrath *et al.* 1999). (a, b) Top and side views of the  $\alpha$ -carbon model of the yeast structure. (c, d) Backbone model of the *E. coli* structure. (d) is rotated by  $90^\circ$  with respect to (c). Black dot in (a) and black lines in (b–d) show the putative rotation axis (Wang & Oster 1998).  $\beta$ -subunits in green and  $\alpha$ -subunits in cyan.

We are grateful to Professor Masasuke Yoshida and the members of CREST Team 13 for collaboration and discussion, and to Dr Eiro Muneyuki for many useful comments. This work was supported in part by Grants-in-Aid from the Ministry of Science, Education, Sports and Culture of Japan, and a Keio University Special Grant-in-Aid. R. Yasuda was a Research Fellow of the Japan Society for the Promotion of Science.

## REFERENCES

- Abrahams, J. P., Leslie, A. G. W., Lutter, R. & Walker, J. E. 1994 Structure at 2.8 Å of F<sub>1</sub>-ATPase from bovine heart mitochondria. *Nature* **370**, 621–628.
- Aggeler, R., Ogilvie, I. & Capaldi, R. A. 1997 Rotation of a  $\gamma$ - $\epsilon$  subunit domain in the *Escherichia coli* F<sub>1</sub> F<sub>0</sub>-ATP synthase complex. *J. Biol. Chem.* **272**, 19 621–19 624.
- Berg, H. C. & Turner, L. 1993 Torque generated by the flagellar motor of *Escherichia coli*. *Biophys. J.* **65**, 2201–2216.
- Block, S. M. 1998 Kinesin: what gives? *Cell* **93**, 5–8.
- Boekema, E. J., Ubbink-Kok, T., Lolkema, J. S., Brisson, A. & Konings, W. N. 1997 Visualization of a peripheral stalk in V-type ATPase: evidence for the stator structure essential to rotational catalysis. *Proc. Natl Acad. Sci. USA* **94**, 14 291–14 293.
- Boekema, E. J., Van Breemen, J. F. L., Brisson, A., Ubbink-Kok, T., Konings, W. N. & Lolkema, J. S. 1999 Connecting stalks in V-type ATPase. *Nature* **401**, 37–38.
- Boyer, P. D. 1993 The binding change mechanism for ATP synthase—some probabilities and possibilities. *Biochim. Biophys. Acta* **1140**, 215–250.
- Boyer, P. D. 1997 The ATP synthase—a splendid molecular machine. *A. Rev. Biochem.* **66**, 717–749.
- Boyer, P. D. 2000 Catalytic site forms and controls in ATP synthase catalysis. *Biochim. Biophys. Acta Bioenergetics*. (In the press.)
- Boyer, P. D. & Kohlbrenner, W. E. 1981 The present status of the binding-change mechanism and its relation to ATP formation by chloroplasts. In *Energy coupling in photosynthesis* (ed. B. R. Selman & S. Selman-Reimer), pp. 231–240. Amsterdam: Elsevier.
- Cross, R. L., Grubmeyer, C. & Penefsky, H. S. 1982 Mechanism of ATP hydrolysis by beef heart mitochondrial ATPase. Rate enhancements resulting from cooperative interactions between multiple catalytic sites. *J. Biol. Chem.* **257**, 12 101–12 105.
- Cunningham, D. & Cross, R. L. 1988 Catalytic site occupancy during ATP hydrolysis by MF<sub>1</sub>-ATPase. Evidence for alternating high affinity site during steady-state turnover. *J. Biol. Chem.* **263**, 18 850–18 856.
- DeRosier, D. J. 1998 The turn of the screw: the bacterial flagellar motor. *Cell* **93**, 17–20.
- Dominguez, R., Freyzon, Y., Trybus, K. M. & Cohen, C. 1998 Crystal structure of a vertebrate smooth myosin motor domain and its complex with the essential light chain: visualization of the pre-power stroke state. *Cell* **94**, 559–571.
- Duncan, T. M., Bulygin, V. V., Zhou, Y., Hutcheon, M. L. & Cross, R. L. 1995 Rotation of subunits during catalysis by *Escherichia coli* F<sub>1</sub>-ATPase. *Proc. Natl Acad. Sci. USA* **92**, 10 964–10 968.
- Fillingame, R. H., Jones, P. C., Jiang, W., Valiyaveetil, F. I. & Dmitriev, O. Y. 1998 Subunit organization and structure in the F<sub>0</sub> sector of *Escherichia coli* F<sub>1</sub>F<sub>0</sub> ATP synthase. *Biochim. Biophys. Acta* **1365**, 135–142.
- Funatsu, T., Harada, Y., Tokunaga, M., Saito, K. & Yanagida, T. 1995 Imaging of single fluorescent molecules and individual ATP turnovers by single myosin molecules in aqueous solution. *Nature* **374**, 555–559.
- Galkin, M. A. & Vinogradov, A. D. 1999 Energy-dependent transformation of the catalytic activities of the mitochondrial F<sub>0</sub>F<sub>1</sub>-ATP synthase. *FEBS Lett.* **448**, 123–126.
- García, J. J. & Capaldi, R. A. 1998 Unisite catalysis without rotation of the  $\gamma$ - $\epsilon$  domain in *Escherichia coli* F<sub>1</sub>-ATPase. *J. Biol. Chem.* **273**, 15 940–15 945.
- Gelles, J. & Landick, R. 1998 RNA polymerase as a molecular motor. *Cell* **93**, 13–16.
- Goldman, Y. E. 1998 Wag the tail: structural dynamics of actomyosin. *Cell* **93**, 1–4.
- Ha, T., Glass, J., Enderle, Th., Chemla, D. S. & Weiss, S. 1998 Hindered rotational diffusion and rotational jumps of single molecules. *Phys. Rev. Lett.* **80**, 2093–2096.
- Häsler, K., Engelbrecht, S. & Junge, W. 1998 Three-stepped rotation of subunits  $\gamma$  and  $\epsilon$  in single molecules of F-ATPase as revealed by polarized, confocal fluorometry. *FEBS Lett.* **426**, 301–304.
- Hausrath, A. C., Grüber, G., Matthews, B. W. & Capaldi, R. A. 1999 Structural features of the  $\gamma$  subunit of the *Escherichia coli* F<sub>1</sub> ATPase revealed by a 4.4-Å resolution map obtained by x-ray crystallography. *Proc. Natl Acad. Sci. USA* **96**, 13 697–13 702.
- Hisabori, T., Kondoh, A. & Yoshida, M. 1999 The  $\gamma$  subunit in chloroplast F<sub>1</sub>-ATPase can rotate in a unidirectional and counter-clockwise manner. *FEBS Lett.* **463**, 35–38.
- Holmes, K. C., Popp, D., Gebhard, W. & Kabsch, W. 1990 Atomic model of the actin filament. *Nature* **347**, 44–49.
- Hunt, A. J., Gittes, F. & Howard, J. 1994 The force exerted by a single kinesin molecule against a viscous load. *Biophys. J.* **67**, 766–781.
- Huxley, A. F. 1957 Muscle structure and theories of contraction. *Progr. Biophys. Biophys. Chem.* **7**, 255–318.
- Junge, W., Lill, H. & Engelbrecht, S. 1997 ATP synthase: an electrochemical transducer with rotatory mechanics. *Trends Biochem. Sci.* **22**, 420–423.
- Kagawa, Y. 1999 Biophysical studies on ATP synthase. *Adv. Biophys.* **36**, 1–25.
- Kaim, G. & Dimroth, P. 1999 ATP synthesis by F-type ATP synthase is obligatorily dependent on the transmembrane voltage. *EMBO J.* **18**, 4118–4127.
- Kato, Y., Sasayama, T., Muneyuki, E. & Yoshida, M. 1995 Analysis of time-dependent change of *Escherichia coli* F<sub>1</sub>-ATPase activity and its relationship with apparent negative cooperativity. *Biochim. Biophys. Acta* **1231**, 275–281.
- Kato-Yamada, Y., Noji, H., Yasuda, R., Kinoshita Jr, K. & Yoshida, M. 1998 Direct observation of the rotation of  $\gamma$  subunit in F<sub>1</sub>-ATPase. *J. Biol. Chem.* **273**, 19 375–19 377.
- Kinoshita Jr, K. 1998 Linear and rotary molecular motors. *Adv. Exp. Med. Biol.* **453**, 5–14.
- Kinoshita Jr, K. 1999 Real time imaging of rotating molecular machines. *FASEB J.* **13**, S201–S208.
- Kinoshita Jr, K., Yasuda, R., Noji, H., Ishiwata, S. & Yoshida, M. 1998 F<sub>1</sub>-ATPase: a rotary motor made of a single molecule. *Cell* **93**, 21–24.
- Kinoshita Jr, K., Yasuda, R. & Noji, H. 2000 F<sub>1</sub>-ATPase: a highly efficient rotary ATP machine. *Essays Biochem.* **35**. (In the press.)
- Kitamura, K., Tokunaga, M., Hikikoshi Iwane, A. & Yanagida, T. 1999 A single myosin head moves along an actin filament with regular steps of 5.3 nanometres. *Nature* **397**, 129–134.
- Läuger, P. 1977 Ion transport and rotation of bacterial flagella. *Nature* **268**, 360–362.
- Livnah, O., Bayer, E. A., Wilchek, M. & Sussman, J. L. 1993 Three-dimensional structures of avidin and the avidin–biotin complex. *Proc. Natl Acad. Sci. USA* **90**, 5076–5080.
- Lohman, T. M., Thorn, K. & Vale, R. 1998 Staying on track: common features of DNA helicases and microtubule motors. *Cell* **93**, 9–12.

- Mandelkow, E. & Johnson, K. A. 1998 The structural and mechanochemical cycle of kinesin. *Trends Biol. Sci.* **23**, 429–433.
- Matsui, T., Muneyuki, E., Honda, M., Allison, W. S., Dou, C. & Yoshida, M. 1997 Catalytic activity of the  $\alpha_3\beta_3\gamma$  complex of  $F_1$ -ATPase without a noncatalytic nucleotide binding site. *J. Biol. Chem.* **272**, 8215–8221.
- Milgrom, Y. M., Murataliev, M. B. & Boyer, P. D. 1998 Bi-site activation occurs with the native and nucleotide-depleted mitochondrial  $F_1$ -ATPase. *Biochem. J.* **330**, 1037–1043.
- Muneyuki, E. & Hirata, H. 1988 Kinetic analysis of proton translocation catalyzed by  $F_0F_1$ ATPase. *FEBS Lett.* **234**, 455–458.
- Noji, H., Yasuda, R., Yoshida, M. & Kinosita Jr, K. 1997 Direct observation of the rotation of  $F_1$ -ATPase. *Nature* **386**, 299–302.
- Noji, H., Häsler, K., Junge, W., Kinosita Jr, K., Yoshida, M. & Engelbrecht, S. 1999 Rotation of *Escherichia coli*  $F_1$ -ATPase. *Biochem. Biophys. Res. Commun.* **260**, 597–599.
- Omote, H., Sambonmatsu, N., Saito, K., Samboingi, Y., Iwamoto-Kihara, A., Yanagida, T., Wada, Y. & Futai, M. 1999 The  $\gamma$ -subunit rotation and torque generation in  $F_1$ -ATPase from wild-type or uncoupled mutant *Escherichia coli*. *Proc. Natl Acad. Sci. USA* **96**, 7780–7784.
- Oosawa, F. & Hayashi, S. 1986 The loose coupling mechanism in molecular machines of living cells. *Adv. Biophys.* **22**, 151–183.
- Oster, G. & Wang, H. 2000 Reverse engineering a protein: the mechanochemistry of ATP synthase. *Biochim. Biophys. Acta*. (In the press.)
- Rastogi, V. K. & Girvin, M. E. 1999 Structural changes linked to proton translocation by subunit *c* of the ATP synthase. *Nature* **402**, 263–268.
- Sabbert, D., Engelbrecht, S. & Junge, W. 1996 Intersubunit rotation in active  $F_1$ -ATPase. *Nature* **381**, 623–625.
- Sambongi, H., Iko, Y., Tanabe, M., Omote, H., Iwamoto-Kihara, A., Ueda, I., Yanagida, T., Wada, Y. & Futai, M. 1999 Mechanical rotation of the *c* subunit oligomer in ATP synthase ( $F_0F_1$ ): direct observation. *Science* **286**, 1722–1724.
- Sase, I., Miyata, H., Ishiwata, S. & Kinosita Jr, K. 1997 Axial rotation of sliding actin filaments revealed by single-fluorophore imaging. *Proc. Natl Acad. Sci. USA* **94**, 5646–5650.
- Shingyoji, C., Higuchi, H., Yoshimura, M., Katayama, E. & Yanagida, T. 1998 Dynein arms are oscillating force generators. *Nature* **393**, 711–714.
- Shirakihara, Y., Leslie, A. G. W., Abrahams, J. P., Walker, J. E., Ueda, T., Sekimoto, Y., Kambara, M., Saika, K., Kagawa, Y. & Yoshida, M. 1997 The crystal structure of the nucleotide-free  $\alpha_3\beta_3$  subcomplex of  $F_1$ -ATPase from the thermophilic *Bacillus* PS3 is a symmetric trimer. *Structure* **5**, 825–836.
- Stock, D., Leslie, A. G. W. & Walker, J. E. 1999 Molecular architecture of the rotary motor in ATP synthase. *Science* **286**, 1700–1705.
- Suzuki, Y., Yasunaga, T., Ohkura, R., Wakabayashi, T. & Sutoh, K. 1998 Swing of the lever arm of a myosin motor at the isomerization and phosphate-release steps. *Nature* **396**, 380–383.
- Taylor, E. W. 1979 Mechanism of actomyosin ATPase and the problem of muscular contraction. *CRC Crit. Rev. Biochem.* **6**, 103–164.
- Tsunoda, S. P., Muneyuki, E., Amano, T., Yoshida, M. & Noji, H. 1999 Cross-linking of two  $\beta$  subunits in the closed conformation in  $F_1$ -ATPase. *J. Biol. Chem.* **274**, 5701–5706.
- Wang, H. & Oster, G. 1998 Energy transduction in the  $F_1$  motor of ATP synthase. *Nature* **396**, 279–282.
- Wang, M. D., Schnitzer, M. J., Yin, H., Landick, R., Gelles, J. & Block, S. M. 1998 Force and velocity measured for single molecules of RNA polymerase. *Science* **282**, 902–907.
- Weber, J., Wilke-Mounts, S., Lee, R. S.-F., Grell, E. & Senior, A. E. 1993 Specific placement of tryptophan in the catalytic sites of *Escherichia coli*  $F_1$ -ATPase provides a direct probe of nucleotide binding: maximal ATP hydrolysis occurs with three sites occupied. *J. Biol. Chem.* **268**, 20 126–20 133.
- Wilkens, S. & Capaldi, R. A. 1998 ATP synthase's second stalk comes into focus. *Nature* **393**, 29.
- Yasuda, R., Noji, H., Kinosita Jr, K. & Yoshida, M. 1998  $F_1$ -ATPase is a highly efficient molecular motor that rotates with discrete 120° steps. *Cell* **93**, 1117–1124.
- Zhou, Y., Duncan, T. M. & Cross, R. L. 1997 Subunit rotation in *Escherichia coli*  $F_0F_1$ -ATP synthase during oxidative phosphorylation. *Proc. Natl Acad. Sci. USA* **94**, 10 583–10 587.

